

Crossing the Validation Crisis: Cross-Validation Reduces Benchmarking Variance Surprisingly Well

Célestin Eve^{1,2} Gaël Varoquaux^{2,3} Thomas Moreau¹

¹MIND Team, Université Paris-Saclay, Inria, CEA, Palaiseau, France

²SODA Team, Inria, Palaiseau, France ³Probabl

celestin.eve@inria.fr

Abstract

Modern machine learning progresses through empirical work, benchmarking new methods to evaluate relative performance. However, the statistical variability inherent to evaluation – exacerbated by the stochastic nature of many algorithms – often makes performance estimation unreliable due to the limited test samples available, leading to a validation crisis in which genuine advances are difficult to discern. In this work, we show that cross-validation improves markedly confidence when evaluating and comparing learning algorithm performances. We introduce the concept of *sample gain*, which quantifies the virtual data augmentation achieved by using multiple cross-validation splits to reduce benchmarking variance. Experiments on both synthetic and real-world datasets (histopathologic scans and NLP fine-tuning) demonstrate that multiple splits can substantially improve the reliability and stability of performance estimates, with diminishing returns often setting in later than expected. We also introduce a procedure to dynamically early-stop cross-validation by estimating from the first few folds if subsequent folds will bring large sample gains. Our findings highlight the value of pushing cross-validation on available samples to achieve robust and reliable benchmarking.

1 Introduction

Machine learning (ML) has evolved into an empirical science, where progress is driven by benchmarking of learning algorithms [Eriksson et al., 2025, Hardt, 2026]. Investigators developing a new algorithm need to assess whether it advances the state of the art, providing evidence of improved performance.

But benchmarking algorithms is inherently variable due to multiple sources of randomness, including data splitting, sample ordering, weight initialization, and hyperparameter optimization [Bouthillier et al., 2021]. This variability can lead to inconsistent algorithm rankings and unreliable inferences about relative effectiveness. For instance, in the Grand Challenge on PatchCamelyon (PCam) for histopathology image classification¹, top-performing algorithms exhibited performances that were statistically indistinguishable, highlighting how close margins can be obscured by noise.

For major application fields, reference benchmarks such as ImageNet for image classification [Deng et al., 2009] or Atari games for reinforcement learning [Bellemare et al., 2013], provide reproducibility.

¹<https://patchcamelyon.grand-challenge.org/evaluation/challenge/leaderboard/>

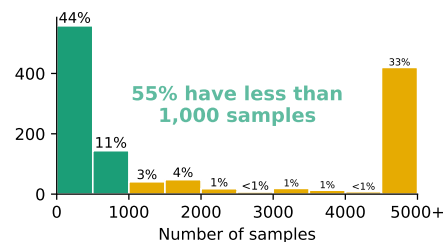


Figure 1: Much ML research hinges on datasets with limited size: size distribution of the 20% most used datasets from OpenML.

Yet, for many domains of ML research such as time series anomaly detection [Sarfraz et al., 2024] or medical imaging [Christodoulou et al., 2024, 2025], custom evaluation processes exacerbate inconsistencies. Addressing these challenges is essential to ensure robust benchmarking practices and progress in ML.

Compounding this issue is the frequent scarcity of data, particularly in domains requiring human labeling, such as natural language processing (text annotation) or medical imaging [Litjens et al., 2017], where limited sample sizes amplify the impact of evaluation variability [Varoquaux, 2018]. Meta-research studies across multiple ML communities provide growing evidence of pervasive small-sample regimes, describing a **validation crisis** in which insufficient data hampers reliable progress [Roberts et al., 2021, Kokol et al., 2022, Chen et al., 2023, Christodoulou et al., 2025]. Much ML and AI research on application domains relies on open datasets with limited sample sizes, some very widely used: more than half of the 20% most used datasets from OpenML have less than 1,000 samples (Figure 1); several representative examples are listed in Table 1.

Recent lines of work have attempted to mitigate the instability of empirical evaluation induced by small-sample regimes. One direction focuses on improving resampling strategies: Nagler et al. [2024]’s asymptotic analysis shows that reshuffled 5-split CV can substantially reduce variance compared to single hold-out evaluations. This motivates the finite-sample question: how much precision do additional splits buy in practice, and when does the extra compute stop paying off? Complementarily, large-scale and continuously updated benchmarks have been proposed to average evaluation noise across datasets and experimental runs, as exemplified by TabArena [Erickson et al., 2025].

Cross-validation (CV) is a classic tool to mitigate benchmarking variability by partitioning the dataset, training and evaluating the algorithm repeatedly, and averaging results to estimate generalization performance [Kohavi, 1995]. By increasing confidence, CV can enhance the reliability of comparisons [Arlot and Celisse, 2010]. Recent evidence also highlights that the choice of validation protocol itself can introduce systematic biases: using simple hold-out validation for model selection can lead to underestimation of performance and favor models with built-in ensembling, whereas nested cross-validation mitigates these effects [Erickson et al., 2025]. However, CV appears underused in modern empirical practice: among the 10,963 studies included in the systematic review of Kolasa et al. [2024] in ML for healthcare from 2010 to 2023, fewer than 14% performed CV. Indeed, CV escalates computational costs, as multiple fits are required per algorithm. This is especially burdensome for complex models like large language models or deep neural networks [Strubell et al., 2019]. CV thus introduces a trade-off between benchmarking variance and cost. Balancing these factors — e.g., choosing the number of folds or splits — is critical for reliable benchmarking.

In this paper, we show that cross-validation substantially improves methods comparison when benchmarking learning algorithms. It brings an **equivalent sample gain** on the statistical power of a machine learning benchmark, which can be very large, reaching values around 10 in our experiments. After giving the theoretical setting, we establish our findings through experiments on synthetic and real data, including histopathologic scans and natural language processing fine-tuning. Our results indicate that **increasing the number of splits exhibits diminishing returns more slowly than**

Table 1: Datasets exemplifying the validation crisis.

Domain	Dataset	Reference	Size	Citations
NLP				
Medical NLP	Rad-QA	Soni et al. 2022	3,074	41
Medical NLP	ACI-Bench	Yim et al. 2023	207	161
Medical NLP	MTS-DIALOG	Ben Abacha et al. 202	1,700	131
Fact-checking	TruthfulQA	Lin et al. 2022	817	3,638
Legal	CUAD	Hendrycks et al. 2021	510	380
Safety	DICES	Aroyo et al. 2023	990	107
Scientific NLP	SciDTB	Yang and Li 2018	1,049	72
Scientific multimodal reasoning	MolPuzzle	Guo et al. 2024	217	39
Medical Imaging				
Medical Decathlon	MSD (10 datasets)	Antonelli et al. 2022	30–750	1,887
Medical Decathlon	MedMNISTv2 (18 datasets)	Yang et al. 2023	780–1,600 (Q1)	1,634
Medical Imaging Survey	29 datasets	Li et al. 2023	12–1,500	115
Others				
Medical NLP & Medical Imaging	MedXpertQA	Zuo et al. 2025	4,460	181
Tabular ML	36 datasets	McElfresh et al. 2023	148–3,000 (median)	402
Tabular ML	111 datasets	Shmuel et al. 2024	43–674 (Q1)	29

anticipated. We also show that **this gain can be partially anticipated from the first few CV-splits**, turning the choice of the number of splits into an explicit statistical and computational trade-off.

2 How to rank? Benchmarking methodology

There are various benchmark settings and goals: evaluation may focus on performance within a single dataset or on robustness across multiple datasets, and may compare either fixed decision functions or learning algorithms, an important distinction that we detail below. While we focus on single-dataset benchmarking, across-dataset benchmarking calls for different statistical methodology [Demšar, 2006]. In this section, we summarize the single-dataset benchmarking methodology and its formal framework in machine learning, and transition to practical resampling estimators.

2.1 Problem setting

A machine-learning problem tackles a task defined on the space $\mathcal{X} \times \mathcal{Y}$, with data (X, Y) drawn from a joint distribution $p_{X,Y}$. Here, X represents the *input* features, typically with $\mathcal{X} = \mathbb{R}^d$ and Y the *output*, which can be discrete *labels* $\mathcal{Y} = \{0, \dots, C - 1\}$ for a C -class classification, or continuous *outcomes* $\mathcal{Y} = \mathbb{R}$ for regression. Let $\ell : \mathcal{Y} \times \mathcal{Y} \rightarrow \mathbb{R}$ be a loss function measuring the quality of a prediction $\hat{y} \in \mathcal{Y}$ compared to a ground truth y . The most common choices are the squared loss ℓ_2 for regression and the error rate for classification. Given a *decision function*—a trained predictor— $g \in \mathcal{Y}^{\mathcal{X}}$, its quality is theoretically measured by the *population risk*:

$$\mathcal{R}^*(g) = \mathbb{E}_{(X,Y) \sim p_{X,Y}} [\ell(g(X), Y)]. \quad (1)$$

Benchmarking trained predictors: Decision functions Benchmarking decision functions strives to rank functions in $\mathcal{Y}^{\mathcal{X}}$ by estimating their relative performance. The *oracle ranking* is the order that respects the population risk \mathcal{R}^* , which we call the *oracle score*. If we evaluate three functions g_i, g_j, g_k where $\mathcal{R}^*(g_k) < \mathcal{R}^*(g_j) < \mathcal{R}^*(g_i)$, the *oracle ranking* is: 1. $g_k \succ 2. g_j \succ 3. g_i$. Note that if the chosen metric is a utility (e.g., R^2 or accuracy), the ranking order is reversed.

In practice, $p_{X,Y}$ is unknown. We instead have access to a dataset $\mathcal{D} \subset \mathcal{X} \times \mathcal{Y}$ sampled from $p_{X,Y}$. We define the empirical score:

$$R_{\mathcal{D}}(g) = \frac{1}{|\mathcal{D}|} \sum_{(x,y) \in \mathcal{D}} \ell(g(x), y). \quad (2)$$

This empirical score is an unbiased estimator of the oracle score: for any sample size m , $\mathbb{E}_{\mathcal{D} \sim p_{X,Y}^{\otimes m}} [R_{\mathcal{D}}(g)] = \mathcal{R}^*(g)$. A ranking is considered robust if the empirical ranking derived from $R_{\mathcal{D}}$ mimics the oracle ranking. The discrepancy between these rankings, caused by evaluating on finite observations rather than the full population, is a primary challenge in benchmarking.

Accounting for training: Benchmarking learning algorithms While the previous section treats decision functions as static objects, in ML these functions are the output of *learning algorithms*. Benchmarking decision functions may suffice for deployment-oriented applications, but the ML research literature studies learning algorithms. Here, good benchmarking is essential for scientific progress, as unstable rankings can propagate misleading conclusions through the literature [Dietterich, 1998]. Learning algorithms can be stochastic, and their performance depends on the data they ingest during training [Bouthillier et al., 2021, Picard, 2021].

Let F_{λ} be a learning algorithm that, for a fixed training size n_{tr} , maps a training set $\mathcal{D}^{\text{tr}} \in (\mathcal{X} \times \mathcal{Y})^{n_{\text{tr}}}$ and other more arbitrary states (such as random inits) $\xi \sim \Xi$ to a decision function $g \in \mathcal{Y}^{\mathcal{X}}$:

$$F_{\lambda} : (\mathcal{D}^{\text{tr}}, \xi) \mapsto g. \quad (3)$$

Here, λ denotes fixed hyper-parameters. The goal of F_{λ} is typically to find a function that approximates the risk minimizer $g^* \in \arg \min_g \mathcal{R}^*(g)$.

To benchmark learning algorithms, we are interested in their *expected* performance across training sets of size n_{tr} sampled from $p_{X,Y}^{\otimes n_{\text{tr}}}$ and internal random states. The underlying question of benchmarking is: which learning algorithm produces better decision functions for a specific task [Dietterich, 1998].

The corresponding *estimand*, or quantity to estimate, is the expected generalization score accounting for these sources of variation:

Definition: Oracle score of a learning algorithm F_λ for training size n_{tr} :

$$\begin{aligned} \mathcal{R}_{n_{\text{tr}}}^*(F_\lambda) &= \mathbb{E}_{\mathcal{D}^{\text{tr}} \sim p_{X,Y}^{\otimes n_{\text{tr}}}} \left[\mathbb{E}_{\xi \sim \Xi} \left[\mathcal{R}^*(F_\lambda(\mathcal{D}^{\text{tr}}, \xi)) \right] \right] \\ &= \mathbb{E}_{\mathcal{D}^{\text{te}} \sim p_{X,Y}^{\otimes n_{\text{te}}}} \left[\mathbb{E}_{\mathcal{D}^{\text{tr}} \sim p_{X,Y}^{\otimes n_{\text{tr}}}} \left[\mathbb{E}_{\xi \sim \Xi} \left[R_{\mathcal{D}^{\text{te}}}(F_\lambda(\mathcal{D}^{\text{tr}}, \xi)) \right] \right] \right]. \end{aligned} \quad (4)$$

Test data
Train data
Internal states

In this formulation, the inner expectation handles internal algorithmic variance (seeds), the middle expectation handles the variance due to the choice of training data of size n_{tr} , and the outer expectation (approximated by a *test set* \mathcal{D}^{te}) evaluates the generalization to the population distribution. This score measures the capacity of the algorithm to consistently produce high-performing predictors.

2.2 Estimation via Resampling

In practice, the oracle score $\mathcal{R}_{n_{\text{tr}}}^*(F_\lambda)$ defined in (4) cannot be computed, as the data-generating distribution $p_{X,Y}$ is unknown and only a single finite dataset $\mathcal{D} = \{(x_i, y_i)\}_{i=1}^n$, with $(x_i, y_i) \stackrel{\text{i.i.d.}}{\sim} p_{X,Y}$ is available. To estimate it, we use resampling methods like *Monte-Carlo Cross-Validation* (MCCV; Picard and Cook 1984), also called *Repeated Random Sub-sampling Validation*, or *ShuffleSplit* in the scikit-learn library [Pedregosa et al., 2011].

A draw $\eta \sim H$ randomly partitions \mathcal{D} into training and test sets $(\mathcal{D}_\eta^{\text{tr}}, \mathcal{D}_\eta^{\text{te}})$, with fixed sizes n_{tr} and n_{te} [Kohavi, 1995]. (4) can then be rewritten as drawing first a total dataset, and then a random split between train and test:

$$\mathcal{R}_{n_{\text{tr}}}^*(F_\lambda) = \mathbb{E}_{\mathcal{D} \sim p_{X,Y}^{\otimes n}} \left[\mathbb{E}_{\eta \sim H} \left[\mathbb{E}_{\xi \sim \Xi} \left[R_{\mathcal{D}_\eta^{\text{te}}}(F_\lambda(\mathcal{D}_\eta^{\text{tr}}, \xi)) \right] \right] \right]. \quad (5)$$

A single hold-out evaluation is defined as:

$$\widehat{R}_{\text{HO}} = R_{\mathcal{D}_\eta^{\text{te}}}(F_\lambda(\mathcal{D}_\eta^{\text{tr}}, \xi)). \quad (6)$$

For K repetitions, we draw i.i.d. splits $(\eta_k)_{k=1}^K$ and randomness $(\xi_k)_{k=1}^K$, and define the MCCV estimator:

$$\widehat{R}_K = \frac{1}{K} \sum_{k=1}^K \underbrace{R_{\mathcal{D}_{\eta_k}^{\text{te}}}(F_\lambda(\mathcal{D}_{\eta_k}^{\text{tr}}, \xi_k))}_{E_k} \quad (7)$$

Here, E_k denotes the evaluation on a single split of the MCCV procedure. Different splits are independent but may overlap, allowing the same observation to appear in the test set multiple times across repetitions. Hence, the variables $(E_k)_{k=1}^K$ are identically distributed but not independent. This dependency dictates the statistical limits of benchmarking.

An Unbiased Estimator with respect to the Estimand Because each split samples a training set of fixed size n_{tr} , MCCV targets exactly the oracle score defined in (4). Formally,

$$\mathbb{E}[\widehat{R}_K] = \mathcal{R}_{n_{\text{tr}}}^*(F_\lambda), \quad (8)$$

as shown by Arlot and Celisse [2010, Eq. 13]. Hence, MCCV is an *unbiased estimator of the oracle score for training size n_{tr}* . This observation is independent of the number of splits; Appendix A translates the source results used in this section to our notation.

Variance of the Estimator The variance of the MCCV estimator reveals a more complex structure. Results from Nadeau and Bengio [2003, Eq. 8] show:

$$\text{Var}[\widehat{R}_K] = \frac{1}{K} \sigma_{\text{HO}}^2 + \frac{K-1}{K} \tau, \quad (9)$$

where $\sigma_{\text{HO}}^2 = \text{Var}[\widehat{R}_{\text{HO}}]$ is the variance of a single hold-out evaluation, and $\tau = \text{Cov}[E_1, E_2] > 0$ quantifies the covariance between evaluations on different splits, *i.e.*, the correlation induced by

reusing observations across splits. As we have $\tau \leq \sigma_{\text{HO}}^2$ (by Cauchy-Schwarz inequality), the variance decreases with K . When the number of repetitions $K \rightarrow \infty$, the first term vanishes, but the second converges to τ . This reveals an irreducible variance component stemming from the finite nature of the dataset: even infinite repetitions cannot reduce variance below τ .

Nadeau and Bengio [2003] show that a *bona fide* estimator (depending only on the data, and no unknown quantities) of $\text{Var}[\hat{R}_K]$ is impossible. To achieve an approximate estimation, Nadeau and Bengio [2003, Sec. 3.1] stipulate that:

$$\tau \approx \frac{n_{\text{te}}}{n_{\text{te}} + n_{\text{tr}}} \sigma_{\text{HO}}^2. \quad (10)$$

Under this approximation, CV appears to hit diminishing returns quickly. With the usual 10–20% test-set recommendation [Kohavi, 1995], a 20% test split gives $\text{Var}[\hat{R}_K] \rightarrow \frac{1}{5} \sigma_{\text{HO}}^2$ as $K \rightarrow \infty$. Rather than interpreting this variance ratio directly, we measure the single-split test-set enlargement needed to match the variance of K -split CV; our experiments show that this equivalent enlargement can be substantial even for practical values of K .

3 A measure of cross-validation efficiency: the *Sample gain*

As shown by eq. (9), the variance of an estimator \hat{R}_K of the oracle score $\mathcal{R}_{n_{\text{tr}}}^*(F_\lambda)$ decreases with the number of repetitions K . To empirically quantify this improvement, we introduce the notion of *sample gain*, to compare the variance of an estimator with K repetitions to the variance of an estimator obtained with a single split (a single hold-out), if we had access to more test data. This quantity can be estimated empirically, provided that we have access to a large enough dataset.

Figure 2 illustrates the evaluation variance of a single-split estimator \hat{R}_{HO} evaluated with an increasingly large test set. It is compared with the evaluation variance of a CV estimator \hat{R}_K evaluated on a fixed test size n_{te} . The *sample gain* quantifies how much larger a single test set would need to be to have the same evaluation variability as the one observed with CV. This measures the virtual augmentation of the test set due to a CV scheme.

Measuring the evaluation noise Let $g = F_\lambda(\mathcal{D}^{\text{tr}}, \xi)$ be the predictor obtained using the data split \mathcal{D}^{tr} and randomness ξ , with fixed training size n_{tr} . We denote by $\hat{R}^*(g)$ an unbiased estimator of the oracle risk $\mathcal{R}^*(g)$, constructed independently of the test set used for evaluation. For a given test set \mathcal{D}^{te} , we can approximate the *estimation error* on this split as:

$$\delta_{\text{HO}} = R_{\mathcal{D}^{\text{te}}}(g) - \hat{R}^*(g). \quad (11)$$

To understand what δ_{HO} measures, consider the variance of the empirical score $R_{\mathcal{D}^{\text{te}}}(g)$. By the Law of Total Variance, we can decompose it into evaluation noise and training instability:

$$\text{Var}[R_{\mathcal{D}^{\text{te}}}(g)] = \underbrace{\mathbb{E}_g [\text{Var}[R_{\mathcal{D}^{\text{te}}}(g) | g]]}_{\text{(A) Expected Evaluation Noise}} + \underbrace{\text{Var}_g [\mathbb{E}[R_{\mathcal{D}^{\text{te}}}(g) | g]]}_{\text{(B) Training Instability}}. \quad (12)$$

Term (B) simplifies to $\text{Var}_g[\mathcal{R}^*(g)]$, quantifying how much the true performance of the algorithm varies across training splits. Term (A) captures the variance of the score around the true risk due to finite test data.

Evaluation-noise approximation Suppose that the expected evaluation noise of the oracle-score estimator $\hat{R}^*(g)$ is negligible compared to that of the test evaluation. In this case,

$$\text{Var}[\delta_{\text{HO}}] \approx \mathbb{E}_g [\text{Var}[R_{\mathcal{D}^{\text{te}}}(g) | g]]. \quad (13)$$

The calculations from eq. (12) to (13) are detailed in Appendix B.

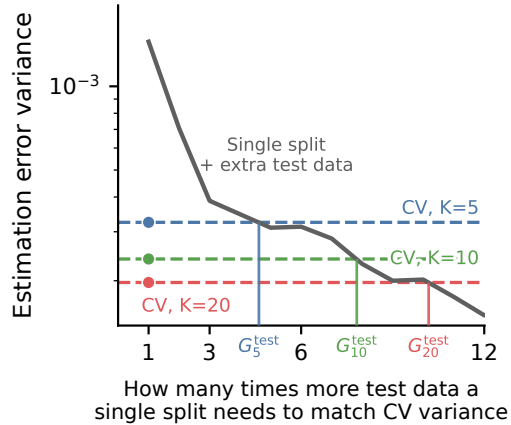


Figure 2: Estimation-error variance behavior and variance-equivalent test sample gain retrievals from one of our real-data experiments. G_K^{test} denotes sample gains for different split counts K as defined in eq. (17).

For the MCCV procedure Let $g_k = F_\lambda(\mathcal{D}_{\eta_k}^{\text{tr}}, \xi_k)$ and define the fold-level benchmark-adjusted error $\delta_k = R_{\mathcal{D}_{\eta_k}^{\text{te}}}(g_k) - \widehat{R}^*(g_k)$. The corresponding K -split estimation error is:

$$\Delta_K = \frac{1}{K} \sum_{k=1}^K \delta_k = \underbrace{\widehat{R}_K}_{\text{CV Estimator}} - \underbrace{\frac{1}{K} \sum_{k=1}^K \widehat{R}^*(g_k)}_{\text{Estimated Oracle Score}}. \quad (14)$$

Similar to the variance decomposition of \widehat{R}_K in eq. (9), the variance of Δ_K follows from the unconditional covariance expansion. Since the fold-level errors $\delta_1, \dots, \delta_K$ are exchangeable under the MCCV split generator, as detailed in [Appendix B](#):

$$\text{Var}[\Delta_K] = \frac{1}{K} \text{Var}[\delta_{\text{HO}}] + \frac{K-1}{K} \tau^{\text{te}}, \quad (15)$$

where $\tau^{\text{te}} = \text{Cov}(\delta_i, \delta_j)$ for $i \neq j$ is the covariance between benchmark-adjusted fold-level test errors. It includes all dependence induced by reusing the finite study sample across MCCV splits, including the fact that a test observation in one split may belong to the training set of another split.

Quantities to measure gains due to cross-validation

Definition 3.1 (Variance-Equivalent Test Size). The variance-equivalent test size N_K^{equiv} of a CV procedure with K splits is defined as is defined as:

$$N_K^{\text{equiv}} = \min \left\{ N' \geq n_{\text{te}} \mid V_1^\delta(N') \leq V_K^\delta(n_{\text{te}}) \right\}. \quad (16)$$

with $V_K^\delta(m)$ the variance of Δ_K when each split uses a test set of size m , computed across independent repetitions; for $K = 1$, $\Delta_1 = \delta_{\text{HO}}$.

Definition 3.2 (Variance-Equivalent Test Sample Gain). The **variance-equivalent test sample gain** of a CV procedure with K splits is defined as:

$$G_K^{\text{test}}(F_\lambda, n_{\text{tr}}) = \frac{N_K^{\text{equiv}}}{n_{\text{te}}}. \quad (17)$$

A value $G_K^{\text{test}}(F_\lambda, n_{\text{tr}}) = 5$ indicates that the variance reduction achieved by K repeated splits is equivalent to evaluating the algorithm on a test set five times larger using a single hold-out. Using the example in [Figure 2](#), the values of variance-equivalent test sample gains for 5, 10 and 20 splits ($G_K^{\text{test}}(F_\lambda, n_{\text{tr}})$ with $K = 5, 10, 20$) can be deducted by looking at the x-values where the variance of the single-split estimator gets lower to the different values of multi-split CV variances.

This notion provides an interpretable measure of the efficiency of cross-validation: it quantifies variance reduction in units of additional evaluation samples, independently of the learning algorithm itself. The covariance-based plug-in estimator and uncertainty estimates used in our figures are detailed in [Section D.1](#).

4 Experimental evaluation of the sample gain

Approximating oracle quantities Estimating the variance of δ_{HO} and Δ_K requires an estimator $\widehat{R}^*(g)$ of $\mathcal{R}^*(g)$ that is independent of the test set and has low evaluation noise. We obtain it from a held-out set much larger than the test set, and decompose the available data into three parts:

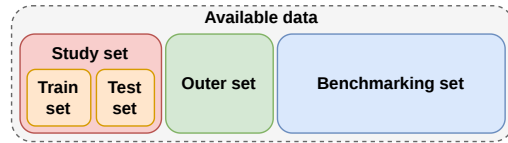


Figure 3: Breakdown and naming of the dataset.

- a *study set* simulates realistic benchmarking conditions; it is repeatedly split into training and test subsets ($\mathcal{D}_i^{\text{tr}}, \mathcal{D}_i^{\text{te}}$) with fixed training size n_{tr} via MCCV;
- an *outer set*, used to independently evaluate $V_1^\delta(m)$ at growing test sizes m ;
- a *benchmarking set* $\mathcal{D}^{\text{bench}}$, large enough to serve as a high-precision oracle estimator $\widehat{R}^*(g) = R_{\mathcal{D}^{\text{bench}}}(g)$.

This decomposition is illustrated in [Figure 3](#). Because $\mathcal{D}^{\text{bench}}$ is much larger than the test set, its evaluation noise is negligible, satisfying the approximation in (13).

Experimental settings We run experiments on synthetic data, medical image classification, and NLP fine-tuning. For the real-world settings, we use very large datasets so that a sizable benchmarking set can be carved out, and restrict study sets to sizes typical of ML benchmarks. Our implementations rely on the Python libraries `scikit-learn` [Pedregosa et al., 2011], `PyTorch` [Paszke et al., 2019] and `Benchopt` [Moreau et al., 2022]. The experimental details are in Appendix E.

Synthetic data As a controlled setting, we use a regression task on synthetic data (the data process described in Appendix E), with a 100,000-sample benchmarking set and n_{te} set to 20% of the study set as per the standard recommendation.

The main runs use `Ridge` [Hoerl and Kennard, 1970], `GradientBoosting` [Friedman, 2001], `ExtraTrees` [Geurts et al., 2006], and a one-hidden-layer MLP. A solver-diversity experiment additionally covers `KNeighbors` [Cover and Hart, 1967], `DecisionTree` [Breiman et al., 1984], `HistGradientBoosting`, and `SVR` [Cortes and Vapnik, 1995], spanning convex estimators, tree ensembles, boosting, local nonparametric regressors, support-vector regression, and a small neural network. It therefore lets us explore how CV sample gains are primarily explained.

Histopathologic scans classification For medical image classification, we use `PatchCameLyon` (PCam; Veeling et al. 2018), from the Camelyon16 Grand Challenge on cancer metastasis detection: 294,912 image patches of size 96×96 extracted from histopathology scans of lymph nodes, labeled by the presence or absence of metastatic tissue.

We evaluate three convolutional neural network architectures: `WideResNet101_2` [Zagoruyko and Komodakis, 2016], `DenseNet121` [Huang et al., 2017], `MobileNetV2` [Sandler et al., 2018], selected based on their reported performance on PCam via the `TIAToolbox` library [Pocock et al., 2022]. Preprocessing pipelines are standardized across architectures, following the same library. We also use the transformer-based `ViT-B/16` [Dosovitskiy et al. 2021].

NLP fine-tuning For NLP, we use `Yelp Review Full` (Yelp; Zhang et al. 2015), a classification benchmark of over 650,000 user reviews labeled with integer ratings from 1 to 5. We fine-tune two transformer architectures: `BERT` [Devlin et al., 2019] and `XLM-RoBERTa` [Conneau et al., 2020], keeping hyperparameters fixed to isolate the effect of the validation strategy.

5 Empirical Results

5.1 Test Sample Gain

Figure 4 presents the variance-equivalent test sample gain results on the simulated linear dataset up to $K = 200$ splits using 100 seeds, at training size $N = 1,000$. `Ridge` presents a variance-equivalent test sample gain of $G_{200}^{\text{test}}(\text{Ridge}, N) \approx 14$: cross-validating the data 200 times conceptually multiplies your test set by 14 in this experimental setup. Considering the MLP, the sample gains goes up to $G_{200}^{\text{test}} = 15$, with diminishing returns settling in after about 80 splits for this learning algorithm, suggesting that CV can yield very important gains with neural networks.

Figure 5 presents the variance-equivalent test sample gain results on the different datasets up to $K = 20$ splits. We observe a general tendency: there is an

important variance-equivalent test sample gain for the vast majority of setups we have run experiments with. Real-data curves are noisier than the simulated ones as the simulated runs are cheaper and could be averaged over many more seeds (cf. Appendix E), but follow the same behavior.

These substantial gains after $K = 5$ splits are persistent in every experimental settings we work on: even for the lowest sample gains of $G_{20}^{\text{test}} = 5$ for `ExtraTrees` and `GradientBoosting` on the simulated pipeline, results had still not converge after $K = 5$ splits. Appendix F shows that our results are not dependent on the CV procedure: repeated K -Folds [Geisser, 1975] yield comparable

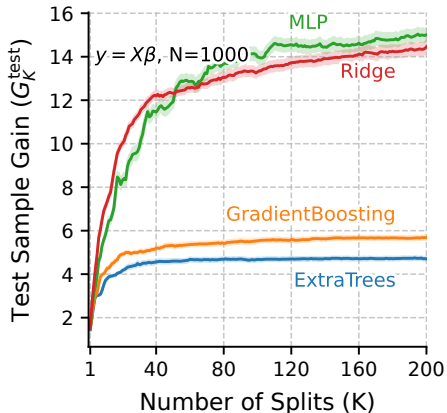


Figure 4: Long-run simulated variance-equivalent test sample gains with 95% confidence intervals after 100 bootstrap resamples over seeds.

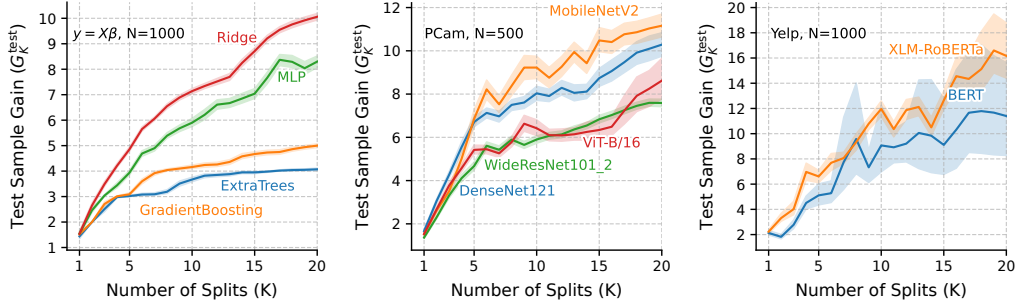


Figure 5: **Variance-equivalent test sample gains** with 95% confidence intervals after 100 bootstrap resamples over seeds.

results. This is at odds with the common heuristics of cross-validating no more than K times when the test size is $\frac{1}{K}$ as each and every sample would have been retrieved in the test set once doing K -fold CV. This leads to the statement that **CV reduces benchmarking variance surprisingly well**.

Measuring how sample gains settle in CV cost scales linearly with K . Knowing when additional splits are not worth computing is therefore a budgeting question, not just a statistical one. As illustrated by Figure 4, some algorithms, such as ExtraTrees or GradientBoosting, are close to their attainable gain at $K = 20$ on the simulated data, whereas Ridge and MLP can continue improving at much larger K , especially in low-training-size regimes. Results from Section 3 suggest that the growth of G_K^{test} is linked with redundancy between split-specific evaluations. To anticipate this behavior without relying on an outer or benchmarking set, Section D.3 defines a study-only redundancy score $\hat{\omega}_K^{\text{study}}(F_\lambda, n_{\text{tr}})$. It is computed from pairs of split-specific predictors, by measuring whether their predictions and losses are similar on study observations shared by their test folds.

High $\hat{\omega}_K^{\text{study}}$ values therefore indicate that additional repetitions mostly average redundant information, making large further sample gains unlikely. Conversely, low values indicate weaker coupling between splits: they do not guarantee a large gain, but they identify settings where continuing CV can still plausibly pay off.

Early stopping cross-validation After only a few splits of a single CV run (in practice, two or three often suffice as in Figure 6), one can compute the redundancy score $\hat{\omega}_K^{\text{study}}$. If it is high, further repetitions are unlikely to bring large additional gains and CV should be early-stopped; if it is low, continuing CV remains worth considering.

A second diagnostic, described in Section D.2, gives a rough approximation of G_K^{test} without requiring an outer benchmarking set.

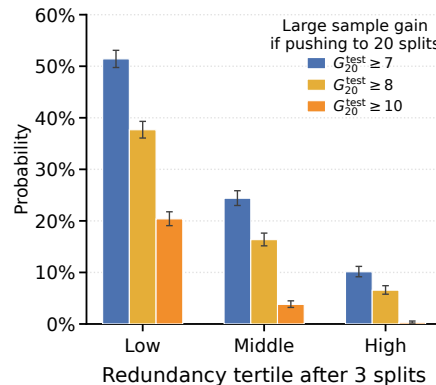


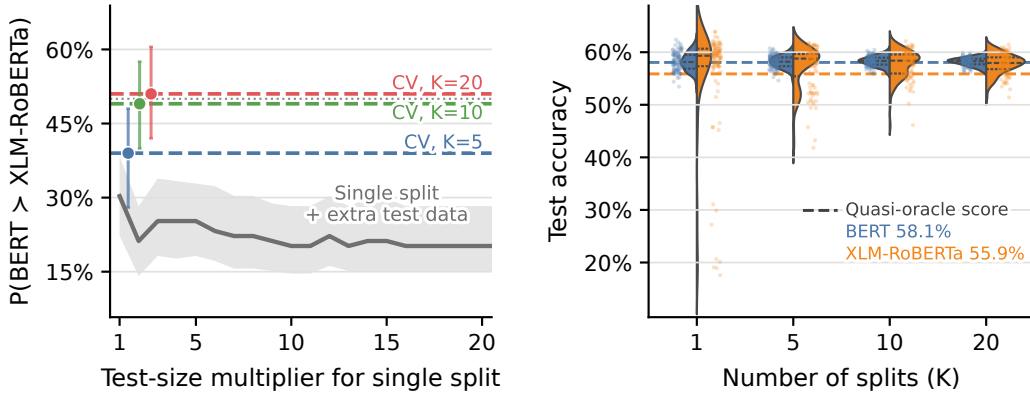
Figure 6: Study-only redundancy as a triage signal for large sample gains.

5.2 Pairwise Ranking

Benchmarks are often interested not only in estimating scores, but in deciding which learning algorithm should be preferred, leading to a ranking problem.

A tempting assumption (common in data science) would be to assume that the oracle ranking is independent of the training size. One could then define a ranking-equivalent sample gain; we detail this view in Appendix H. In our real-data experiments, however, the ranking can depend on the training size. We therefore evaluate rankings separately for each training size.

For each algorithm, we estimate its oracle score at a given training size by averaging its benchmarking-set score over single-split seeds. This defines a *quasi-oracle ranking*. We then test whether pairwise score differences are statistically significant; details are given in Appendix G. The results in Table G.1 show that **multi-split CV retrieves the quasi-oracle ranking more reliably than a single hold-out** when the benchmarking gap is statistically significant.



(a) Proportion of retrieval of the quasi-oracle ranking $\text{BERT} > \text{XLM-RoBERTa}$.

(b) Per-seed test-score distributions.

Figure 7: Pairwise ranking on Yelp at training size $N = 3,000$ with 95% confidence intervals on the left plot after 100 bootstrap resamples over seeds.

Ranking means is not the same as averaging rankings. Our experiments on NLP also demonstrate another beneficial effect of CV over single-split ranking. Using Yelp with $N = 3,000$, the mean benchmarking score of BERT is higher than that of XLM-RoBERTa. Yet single-split evaluations rank XLM-RoBERTa above BERT in roughly 70%–80% of runs, even with augmented test data (Figure 7a).

The reason is visible in Figure 7b: XLM-RoBERTa has severe low-score outliers. These learning failures lower its mean performance, although it often wins on individual splits. As K increases, CV includes these failures and estimates **the ranking of mean scores rather than the mean split-wise ranking**. At $K = 20$, the retrieval proportion is close to balanced, consistently with Table G.1: the difference between BERT and XLM-RoBERTa at $N = 3,000$ is not statistically significant.

6 Conclusion

Our work shows that cross-validation can make machine-learning benchmarks much more reliable in small-data regimes. Through the variance-equivalent test sample gain, we quantify benefits of cross-validation in interpretable units: the amount of additional test data a single-split evaluation would need to reach comparable stability. Across synthetic regression, histopathology image classification, and NLP fine-tuning, repeated validation splits yield substantial gains, often far beyond the first few splits and the classic heuristic that each observation only needs to be held out once.

These gains are not uniform across algorithms. Some methods lead to benchmarks that settle quickly, whereas others keep benefiting from many more repetitions. We therefore introduce a study-only redundancy statistic, computable after only a few splits of a single CV run. High redundancy indicates that further repetitions are unlikely to bring large additional gains, while low redundancy suggests that continuing CV may remain worthwhile.

Our results also show that multi-split CV improves algorithm ranking when benchmarking differences are statistically meaningful, and can expose learning failures hidden by single splits. Thus, when benchmark data are limited and comparisons are close, single train/test splits should be avoided. Practitioners should use multi-split CV when computationally feasible, and rely on early redundancy diagnostics to decide whether larger K is worth the cost.

Limitations remain: because our protocol requires large benchmarking sets, our real-data experiments are constrained by dataset availability and computational cost, and cover only two domains. Broader benchmarking would help ground our results across application-specific domains, while our methodological work lays the foundation for such comparisons. As automated systems have growing societal impact, rigorous algorithm selection is particularly critical in small-sample domains such as medical imaging. We contribute by making empirical comparisons more stable and uncertainty-aware.

Acknowledgements

We thank Shan Raza, lead developer of TIAToolbox, for sharing with us the code used for training the pre-trained models of the library, which helped us in the experiments run on the PatchCamelyon dataset. This research was supported in part by the French National Research Agency (ANR) through the BenchArk project (ANR-24-IAS2-0003) as well as Hi! PARIS and ANR/France 2030 program (ANR-23-IACL-0005).

References

- Michela Antonelli, Annika Reinke, Spyridon Bakas, Keyvan Farahani, Annette Kopp-Schneider, Bennett A. Landman, Geert Litjens, Bjoern Menze, Olaf Ronneberger, Ronald M. Summers, Bram van Ginneken, Michel Bilello, Patrick Bilic, Patrick F. Christ, Richard K. G. Do, Marc J. Gollub, Stephan H. Heckers, Henkjan Huisman, William R. Jarnagin, Maureen K. McHugo, Sandy Napel, Jennifer S. Golia Pernicka, Kawal Rhode, Catalina Tobon-Gomez, Eugene Vorontsov, James A. Meakin, Sebastien Ourselin, Manuel Wieserfarth, Pablo Arbeláez, Byeonguk Bae, Sihong Chen, Laura Daza, Jianjiang Feng, Baochun He, Fabian Isensee, Yuanfeng Ji, Fucang Jia, Ildoo Kim, Klaus Maier-Hein, Dorit Merhof, Akshay Pai, Beomhee Park, Mathias Perslev, Ramin Rezaifar, Oliver Rippel, Ignacio Sarasua, Wei Shen, Jaemin Son, Christian Wachinger, Liansheng Wang, Yan Wang, Yingda Xia, Daguang Xu, Zhanwei Xu, Yefeng Zheng, Amber L. Simpson, Lena Maier-Hein, and M. Jorge Cardoso. The Medical Segmentation Decathlon. *Nature Communications*, 13(1):4128, 2022.
- Sylvain Arlot and Alain Celisse. A survey of cross-validation procedures for model selection. *Statistics Surveys*, 4:40–79, 2010.
- Lora Aroyo, Alex Taylor, Mark Díaz, Christopher Homan, Alicia Parrish, Gregory Serapio-García, Vinodkumar Prabhakaran, and Ding Wang. DICES Dataset: Diversity in Conversational AI Evaluation for Safety. In *Advances in Neural Information Processing Systems (NeurIPS)*, 2023.
- Marc G. Bellemare, Yavar Naddaf, Joel Veness, and Michael Bowling. The Arcade Learning Environment: An Evaluation Platform for General Agents. *Journal of Artificial Intelligence Research*, 47:253–279, 2013.
- Asma Ben Abacha, Wen-wai Yim, Yadan Fan, and Thomas Lin. An Empirical Study of Clinical Note Generation from Doctor–Patient Encounters. In *Conference of the European Chapter of the Association for Computational Linguistics (EACL)*, 2023.
- Yoshua Bengio and Yves Grandvalet. No Unbiased Estimator of the Variance of K-Fold Cross-Validation. *Journal of Machine Learning Research (JMLR)*, 5:1089–1105, 2004.
- Xavier Bouthillier, Pierre Delaunay, Mirko Bronzi, Assya Trofimov, Brennan Nichyporuk, Justin Szeto, Nazanin Mohammadi Sepahvand, Edward Raff, Kanika Madan, Vikram Voleti, Samira Ebrahimi Kahou, Vincent Michalski, Dmitriy Serdyuk, Tal Arbel, Chris Pal, Gael Varoquaux, and Pascal Vincent. Accounting for Variance in Machine Learning Benchmarks. In *Proceedings of Machine Learning and Systems*, volume 3, pages 747–769, 2021.
- Leo Breiman, J. H. Friedman, Richard A. Olshen, and C. J. Stone. *Classification and Regression Trees*. Wadsworth, 1984. ISBN 0-534-98053-8.
- Zhiyi Chen, Bowen Hu, Xuerong Liu, Benjamin Becker, Simon B. Eickhoff, Kuan Miao, Xingmei Gu, Yancheng Tang, Xin Dai, Chao Li, Artemiy Leonov, Zhibing Xiao, Zhengzhi Feng, Ji Chen, and Hu Chuan-Peng. Sampling inequalities affect generalization of neuroimaging-based diagnostic classifiers in psychiatry. *BMC Medicine*, 21(1):241, 2023.
- Evangelia Christodoulou, Annika Reinke, Rola Houhou, Piotr Kalinowski, Selen Erkan, Carole H. Sudre, Ninon Burgos, Sofiène Boutaj, Sophie Loizillon, Maëlys Solal, Nicola Rieke, Veronika Cheplygina, Michela Antonelli, Leon D. Mayer, Minu D. Tizabi, M. Jorge Cardoso, Amber Simpson, Paul F. Jäger, Annette Kopp-Schneider, Gaël Varoquaux, Olivier Colliot, and Lena Maier-Hein. Confidence Intervals Uncovered: Are We Ready for Real-World Medical Imaging AI? In *Medical Image Computing and Computer Assisted Intervention (MICCAI)*. Springer, 2024.

- Evangelia Christodoulou, Annika Reinke, Pascaline Andr , Patrick Godau, Piotr Kalinowski, Rola Houhou, Selen Erkan, Carole H. Sudre, Ninon Burgos, Sofi ne Boutaj, Sophie Loizillon, Ma lysolal, Veronika Cheplygina, Charles Heitz, Michal Kozubek, Michela Antonelli, Nicola Rieke, Antoine Gilson, Leon D. Mayer, Minu D. Tizabi, M. Jorge Cardoso, Amber Simpson, Annette Kopp-Schneider, Ga l Varoquaux, Olivier Colliot, and Lena Maier-Hein. False Promises in Medical Imaging AI? Assessing Validity of Outperformance Claims. *arXiv preprint arXiv:2505.04720*, 2025.
- Alexis Conneau, Kartikay Khandelwal, Naman Goyal, Vishrav Chaudhary, Guillaume Wenzek, Francisco Guzm n, Edouard Grave, Myle Ott, Luke Zettlemoyer, and Veselin Stoyanov. Unsupervised Cross-lingual Representation Learning at Scale. In *Annual Meeting of the Association for Computational Linguistics (ACL)*, 2020.
- Corinna Cortes and Vladimir Vapnik. Support-vector networks. *Machine Learning*, 20(3):273–297, 1995.
- Thomas M. Cover and Peter E. Hart. Nearest neighbor pattern classification. *IEEE Transactions on Information Theory*, 13(1):21–27, 1967.
- Janez Dem sar. Statistical Comparisons of Classifiers over Multiple Data Sets. *Journal of Machine Learning Research (JMLR)*, 7(1):1–30, 2006.
- Jia Deng, Wei Dong, Richard Socher, Li-Jia Li, Kai Li, and Li Fei-Fei. ImageNet: A Large-Scale Hierarchical Image Database. In *Conference on Computer Vision and Pattern Recognition (CVPR)*, 2009.
- Jacob Devlin, Ming-Wei Chang, Kenton Lee, and Kristina Toutanova. BERT: Pre-training of Deep Bidirectional Transformers for Language Understanding. In *Proceedings of NAACL-HLT 2019*, pages 4171–4186, 2019.
- Thomas G. Dietterich. Approximate Statistical Tests for Comparing Supervised Classification Learning Algorithms. *Neural Computation*, 10(7):1895–1923, 1998.
- Alexey Dosovitskiy, Lucas Beyer, Alexander Kolesnikov, Dirk Weissenborn, Xiaohua Zhai, Thomas Unterthiner, Mostafa Dehghani, Matthias Minderer, Georg Heigold, Sylvain Gelly, Jakob Uszkoreit, and Neil Houlsby. An Image is Worth 16x16 Words: Transformers for Image Recognition at Scale. In *Proceedings of the 9th International Conference on Learning Representations (ICLR)*, 2021.
- Nick Erickson, Lennart Purucker, Andrej Tschalzev, David Holzm ller, Prateek Mutalik Desai, David Salinas, and Frank Hutter. TabArena: A Living Benchmark for Machine Learning on Tabular Data. In *Advances in Neural Information Processing Systems (NeurIPS) – Datasets and Benchmarks Track*, 2025.
- Maria Eriksson, Erasmo Purificato, Arman Noroozian, Joao Vinagre, Guillaume Chaslot, Emilia Gomez, and David Fernandez-Llorca. Can We Trust AI Benchmarks? An Interdisciplinary Review of Current Issues in AI Evaluation. In *Proceedings of the AAAI/ACM Conference on AI, Ethics, and Society*, volume 8, pages 850–864, 2025.
- Jerome H. Friedman. Greedy Function Approximation: A Gradient Boosting Machine. *The Annals of Statistics*, 29(5):1189–1232, 2001.
- Seymour Geisser. The Predictive Sample Reuse Method with Applications. *Journal of the American Statistical Association*, 70(350):320–328, 1975.
- Pierre Geurts, Damien Ernst, and Louis Wehenkel. Extremely randomized trees. *Machine Learning*, 63(1):3–42, 2006.
- Kehan Guo, Bozhao Nan, Yujun Zhou, Taicheng Guo, Zhichun Guo, Mihir Surve, Zhenwen Liang, Nitesh V. Chawla, Olaf Wiest, and Xiangliang Zhang. Can LLMs Solve Molecule Puzzles? A Multimodal Benchmark for Molecular Structure Elucidation. In *Advances in Neural Information Processing Systems (NeurIPS) – Datasets and Benchmarks Track*, 2024.
- Moritz Hardt. *The Emerging Science of Machine Learning Benchmarks*. Princeton University Press, 2026.

- Dan Hendrycks, Collin Burns, Anya Chen, and Spencer Ball. CUAD: An Expert-Annotated NLP Dataset for Legal Contract Review. In *Advances in Neural Information Processing Systems (NeurIPS) – Datasets and Benchmarks Track*, 2021.
- Arthur E. Hoerl and Robert W. Kennard. Ridge Regression: Biased Estimation for Nonorthogonal Problems. *Technometrics*, 12(1):55–67, 1970.
- Gao Huang, Zhuang Liu, Laurens Van Der Maaten, and Kilian Q. Weinberger. Densely Connected Convolutional Networks. In *Conference on Computer Vision and Pattern Recognition (CVPR)*, 2017.
- Diederik P. Kingma and Jimmy Ba. Adam: A Method for Stochastic Optimization. In *Proceedings of the 3rd International Conference on Learning Representations (ICLR)*, 2015.
- Ron Kohavi. A Study of Cross-Validation and Bootstrap for Accuracy Estimation and Model Selection. In *International Joint Conference on Artificial Intelligence (IJCAI)*, 1995.
- Peter Kokol, Marko Kokol, and Sašo Zagoranski. Machine learning on small size samples: A synthetic knowledge synthesis. *Science Progress*, 105(1):00368504211029777, 2022.
- Katarzyna Kolasa, Bisrat Admassu, Malwina Hołownia-Voloskova, Katarzyna J. Kędzior, Jean-Etienne Poirrier, and Stefano Perni. Systematic reviews of machine learning in healthcare: a literature review. *Expert Review of Pharmacoeconomics & Outcomes Research*, 24(1):63–115, 2024.
- Quentin Lhoest, Albert Villanova del Moral, Yacine Jernite, Abhishek Thakur, Patrick von Platen, Suraj Patil, Julien Chaumond, Mariama Drame, Julien Plu, Lewis Tunstall, Joe Davison, Mario Šaško, Gunjan Chhablani, Bhavitvya Malik, Simon Brandeis, Teven Le Scao, Victor Sanh, Canwen Xu, Nicolas Patry, Angelina McMillan-Major, Philipp Schmid, Sylvain Gugger, Clément Delangue, Théo Matussière, Lysandre Debut, Stas Bekman, Pierric Cistac, Thibault Goehringer, Victor Mustar, François Lagunas, Alexander M. Rush, and Thomas Wolf. Datasets: A Community Library for Natural Language Processing. In *Conference on Empirical Methods in Natural Language Processing: System Demonstrations*, 2021.
- Johann Li, Guangming Zhu, Cong Hua, Mingtao Feng, Basheer Bennamoun, Ping Li, Xiaoyuan Lu, Juan Song, Peiyi Shen, Xu Xu, Lin Mei, Liang Zhang, Syed Shah, and Mohammed Bennamoun. A Systematic Collection of Medical Image Datasets for Deep Learning. *ACM Computing Surveys*, 56, 2023.
- Stephanie Lin, Jacob Hilton, and Owain Evans. TruthfulQA: Measuring How Models Mimic Human Falsehoods. In *Annual Meeting of the Association for Computational Linguistics (ACL)*, 2022.
- Geert Litjens, Thijs Kooi, Babak Ehteshami Bejnordi, Arnaud Arindra Adiyoso Setio, Francesco Ciompi, Mohsen Ghafoorian, Jeroen van der Laak, Bram van Ginneken, and Clara I. Sánchez. A Survey on Deep Learning in Medical Image Analysis. *Medical Image Analysis*, 42:60–88, 2017.
- Ilya Loshchilov and Frank Hutter. Decoupled Weight Decay Regularization. In *Proceedings of the 7th International Conference on Learning Representations (ICLR)*, 2019.
- Sébastien Marcel and Yann Rodriguez. Torchvision the machine-vision package of torch. In *Proceedings of the 18th ACM International Conference on Multimedia*, 2010.
- Duncan McElfresh, Sujay Khandagale, Jonathan Valverde, Vishak Prasad C., Ganesh Ramakrishnan, Micah Goldblum, and Colin White. When Do Neural Nets Outperform Boosted Trees on Tabular Data? In *Advances in Neural Information Processing Systems (NeurIPS)*, 2023.
- Thomas Moreau, Mathurin Massias, Alexandre Gramfort, Pierre Ablin, Pierre-Antoine Bannier, Benjamin Charlier, Mathieu Dagréou, Tom Dupré La Tour, Ghislain Durif, Cássio F. Dantas, Quentin Klopfenstein, Johan Larsson, En Lai, Tanguy Lefort, Benoît Malézieux, Badr Moufad, Binh T. Nguyen, Alain Rakotomamonjy, Zaccharie Ramzi, Joseph Salmon, and Samuel Vaiter. Benchopt: Reproducible, efficient and collaborative optimization benchmarks. In *Advances in Neural Information Processing Systems (NeurIPS)*, 2022.

- Claude Nadeau and Yoshua Bengio. Inference for the Generalization Error. *Machine Learning*, 52(3):239–281, 2003.
- Thomas Nagler, Lennart Schneider, Bernd Bischl, and Matthias Feurer. Reshuffling Resampling Splits Can Improve Generalization of Hyperparameter Optimization. In *Advances in Neural Information Processing Systems (NeurIPS)*, 2024.
- Adam Paszke, Sam Gross, Francisco Massa, Adam Lerer, James Bradbury, Gregory Chanan, Trevor Killeen, Zeming Lin, Natalia Gimelshein, Luca Antiga, et al. Pytorch: An Imperative Style, High-Performance Deep Learning Library. In *Advances in Neural Information Processing Systems (NeurIPS)*, 2019.
- Fabian Pedregosa, Gael Varoquaux, Alexandre Gramfort, Vincent Michel, Bertrand Thirion, Olivier Grisel, Mathieu Blondel, Peter Prettenhofer, Ron Weiss, Vincent Dubourg, Jake Vanderplas, Alexandre Passos, David Cournapeau, Matthieu Brucher, Matthieu Perrot, and Edouard Duchesnay. Scikit-learn: Machine Learning in Python. *Journal of Machine Learning Research (JMLR)*, 12: 2825–2830, 2011.
- David Picard. Torch. manual_seed (3407) is all you need: On the influence of random seeds in deep learning architectures for computer vision. *arXiv preprint arXiv:2109.08203*, 2021.
- Richard R. Picard and R. Dennis Cook. Cross-validation of Regression Models. *Journal of the American Statistical Association*, 79(387):575–583, 1984.
- Johnathan Pocock, Simon Graham, Quoc Dang Vu, Mostafa Jahanifar, Srijay Deshpande, Giorgos Hadjigeorgiou, Adam Shephard, Raja Muhammad Saad Bashir, Mohsin Bilal, Wenqi Lu, et al. TIAToolbox as an end-to-end library for advanced tissue image analytics. *Communications Medicine*, 2(1):120, 2022.
- Michael Roberts, Derek Driggs, Matthew Thorpe, Julian Gilbey, Michael Yeung, Stephan Ursprung, Angelica I. Aviles-Rivero, Christian Etmann, Cathal McCague, Lucian Beer, Jonathan R. Weir-McCall, Zhongzhao Teng, Effrossyni Gkrania-Klotsas, James H. F. Rudd, Evis Sala, and Carola-Bibiane Schönlieb. Common pitfalls and recommendations for using machine learning to detect and prognosticate for COVID-19 using chest radiographs and CT scans. *Nature Machine Intelligence*, 3(3):199–217, 2021.
- Mark Sandler, Andrew Howard, Menglong Zhu, Andrey Zhmoginov, and Liang-Chieh Chen. MobileNetV2: Inverted Residuals and Linear Bottlenecks. In *Conference on Computer Vision and Pattern Recognition (CVPR)*, 2018.
- M. Saquib Sarfraz, Mei-Yen Chen, Lukas Layer, Kunyu Peng, and Marios Koulakis. Position: Quo Vadis, Unsupervised Time Series Anomaly Detection? In *International Conference on Machine Learning (ICML)*, 2024.
- Assaf Shmuel, Oren Glickman, and Teddy Lazebnik. A Comprehensive Benchmark of Machine and Deep Learning Across Diverse Tabular Datasets. *arXiv preprint arXiv:2408.14817*, 2024.
- Sarvesh Soni, Meghana Gudala, Atieh Pajouhi, and Kirk Roberts. RadQA: A Question Answering Dataset to Improve Comprehension of Radiology Reports. In *Proceedings of the Thirteenth Language Resources and Evaluation Conference*. European Language Resources Association (ELRA), 2022.
- Emma Strubell, Ananya Ganesh, and Andrew McCallum. Energy and Policy Considerations for Deep Learning in NLP. In *Annual Meeting of the Association for Computational Linguistics (ACL)*, 2019.
- Gaël Varoquaux. Cross-validation failure: Small sample sizes lead to large error bars. *NeuroImage*, 180:68–77, 2018.
- Bastiaan S. Veeling, Jasper Linmans, Jim Winkens, Taco Cohen, and Max Welling. Rotation Equivariant CNNs for Digital Pathology. In *Medical Image Computing and Computer Assisted Intervention (MICCAI)*. Springer, 2018.

- An Yang and Sujian Li. SciDTB: Discourse Dependency TreeBank for Scientific Abstracts. In *Annual Meeting of the Association for Computational Linguistics (ACL)*, 2018.
- Jiancheng Yang, Rui Shi, Donglai Wei, Zequan Liu, Lin Zhao, Bilian Ke, Hanspeter Pfister, and Bingbing Ni. MedMNIST v2 – A large-scale lightweight benchmark for 2D and 3D biomedical image classification. *Scientific Data*, 10(1):41, 2023.
- Wen-wai Yim, Yajuan Fu, Asma Ben Abacha, Neal Snider, Thomas Lin, and Meliha Yetisgen. ACI-Bench: A Novel Ambient Clinical Intelligence Dataset for Benchmarking Automatic Visit Note Generation. *Scientific Data*, 10(1):586, 2023.
- Sergey Zagoruyko and Nikos Komodakis. Wide Residual Networks. In *Proceedings of the British Machine Vision Conference (BMVC)*, 2016.
- Xiang Zhang, Junbo Zhao, and Yann LeCun. Character-level Convolutional Networks for Text Classification. In *Advances in Neural Information Processing Systems (NeurIPS)*, 2015.
- Yuxin Zuo, Shang Qu, Yifei Li, Zhangren Chen, Xuekai Zhu, Ermo Hua, Kaiyan Zhang, Ning Ding, and Bowen Zhou. MedXpertQA: Benchmarking Expert-Level Medical Reasoning and Understanding. *arXiv preprint arXiv:2501.18362*, 2025.

A Derivation of Benchmarking Statistics

A.1 Unbiasedness of the CV Estimator [Arlot and Celisse, 2010]

Original Formulation Arlot and Celisse [2010] establish the unbiasedness of the cross-validation estimator in their Equation (13) as follows:

$$\mathbb{E} \left[\widehat{\mathcal{L}}^{\text{CV}} \left(\mathcal{A}; D_n; \left(I_j^{(t)} \right)_{1 \leq j \leq B} \right) \right] = \mathbb{E} [\mathcal{L}_P(\mathcal{A}(D_{n_t}))]. \quad (\text{Arlot \& Celisse, Eq. 13})$$

Original Notation:

- $\widehat{\mathcal{L}}^{\text{CV}}$: The Cross-Validation estimator of the risk.
- \mathcal{A} : The learning algorithm.
- D_n : The full dataset of size n .
- $(I_j^{(t)})_{1 \leq j \leq B}$: The sequence of B training set indices (splits).
- n_t : The size of the training set (cardinality of $I_j^{(t)}$).
- \mathcal{L}_P : The population risk (loss).
- D_{n_t} : A training set of size n_t .

Translation to Our Notation Mapping the components $B \rightarrow K$, $n_t \rightarrow n_{\text{tr}}$, and $\mathcal{A} \rightarrow F_\lambda$, this confirms that the expectation of our MCCV estimator corresponds to the Oracle Score for the specific training size n_{tr} :

$$\mathbb{E}[\widehat{R}_K] = \mathcal{R}_{n_{\text{tr}}}^*(F_\lambda). \quad (\text{A.1})$$

A.2 Variance of the CV Estimator [Nadeau and Bengio, 2003]

Original Formulation Nadeau and Bengio [2003] derive the variance of the average estimator over J splits in their Equation (8). Omitting the specific sample-size scaling factor $\frac{n_2}{n_1}$ used in their specific loss definition for clarity, the structural variance decomposition is:

$$\text{Var}[\widehat{\mu}_J] = \sigma_1 \left(\rho + \frac{1 - \rho}{J} \right). \quad (\text{Nadeau \& Bengio, Eq. 8})$$

Original Notation:

- $\widehat{\mu}_J$: The average estimator over J splits.
- J : The number of repetitions (splits).
- σ_1 : The variance of the estimator on a single split.
- ρ : The correlation coefficient between the estimators of two different splits.

Translation to Our Notation We substitute $J \rightarrow K$, $\widehat{\mu}_J \rightarrow \widehat{R}_K$, and $\sigma_1 \rightarrow \sigma_{\text{HO}}^2$. We also identify the covariance $\tau = \rho \sigma_{\text{HO}}^2$. Expanding the terms yields the decomposition into reducible error (scaled by $1/K$) and irreducible covariance:

$$\text{Var}[\widehat{R}_K] = \sigma_{\text{HO}}^2 \left(\frac{\tau}{\sigma_{\text{HO}}^2} + \frac{1}{K} \left(1 - \frac{\tau}{\sigma_{\text{HO}}^2} \right) \right) = \frac{1}{K} \sigma_{\text{HO}}^2 + \frac{K-1}{K} \tau. \quad (\text{A.2})$$

A.3 Asymptotic Variance under Reshuffling [Nagler et al., 2024]

Original Formulation Nagler et al. [2024] establish the limiting distribution of the estimation error in their Theorem 2.1:

$$\sqrt{n} (\widehat{\mu}(\lambda_j) - \mu(\lambda_j))_{j=1}^J \xrightarrow{d} \mathcal{N}(0, \Sigma), \quad (\text{Nagler et al., Thm 2.1})$$

where the covariance matrix Σ is defined by:

$$\Sigma_{i,j} = \tau_{i,j,M} K(\lambda_i, \lambda_j) \quad (\text{A.3})$$

Original Notation:

- n : The size of the observed dataset.
- $\widehat{\mu}(\lambda_j)$: The M -split validation loss for configuration λ_j .
- $\mu(\lambda_j)$: The true generalization error (population risk).
- J : The number of hyperparameter configurations evaluated.
- $\tau_{i,j,M}$: A term quantifying the overlap probability of validation indices between configurations i and j .
- $K(\lambda_i, \lambda_j)$: The asymptotic covariance between losses for two fixed configurations.

Translation to Our Notation While Nagler et al. [2024] frame their analysis around optimizing over a set of hyperparameter configurations $\{\lambda_1, \dots, \lambda_J\}$, this mathematical framework applies identically to benchmarking a discrete set of fixed learning algorithms $\{F_1, \dots, F_J\}$. Evaluating two different hyperparameter configurations in their setting is equivalent to evaluating two different learning algorithms in ours.

By making the substitution $M \rightarrow K$ (number of splits), mapping λ_j to the j -th learning algorithm F_j , replacing the population risk $\mu(\lambda_j)$ with our oracle score $\mathcal{R}_{n_{\text{tr}}}^*(F_j)$, and replacing the M -split validation loss $\widehat{\mu}(\lambda_j)$ with our MCCV estimator $\widehat{R}_K(F_j)$, Theorem 2.1 can be rewritten for our benchmarking context:

$$\sqrt{n} \left(\widehat{R}_K(F_j) - \mathcal{R}_{n_{\text{tr}}}^*(F_j) \right)_{j=1}^J \xrightarrow{d} \mathcal{N}(0, \Sigma) . \quad (\text{A.4})$$

The asymptotic covariance matrix Σ provides the formal foundation for the variance reduction we observe. In this setting, $\Sigma_{i,j}$ describes how the evaluation errors of two algorithms F_i and F_j covary:

$$\Sigma_{i,j} = \rho_{\text{overlap}} \cdot \sigma_{\text{HO}}^2(F_i, F_j) . \quad (\text{A.5})$$

Here, $\sigma_{\text{HO}}^2(F_i, F_j)$ is the asymptotic covariance between the losses of the two algorithms on a single random test point. The crucial factor is ρ_{overlap} , which represents the probability of overlap in validation indices between the evaluations of F_i and F_j (i.e., the proportion of test samples in MCCV).

B Measuring and approximating the evaluation noise: the justification of Sample Gain

Single-split benchmark-adjusted error. Let $g = F_\lambda(\mathcal{D}^{\text{tr}}, \xi)$ be the predictor obtained from a training set \mathcal{D}^{tr} and algorithmic randomness ξ , with fixed training size n_{tr} . We denote by $\widehat{R}^*(g)$ an unbiased estimator of the oracle risk $\mathcal{R}^*(g)$, constructed independently of the test set used for evaluation. For a held-out test set \mathcal{D}^{te} , define the single-split benchmark-adjusted *estimation error*:

$$\delta_{\text{HO}} = R_{\mathcal{D}^{\text{te}}}(g) - \widehat{R}^*(g) . \quad (\text{B.1})$$

To understand what δ_{HO} measures, consider the variance of the empirical score $R_{\mathcal{D}^{\text{te}}}(g)$. By the law of total variance,

$$\text{Var}[R_{\mathcal{D}^{\text{te}}}(g)] = \underbrace{\mathbb{E}_g[\text{Var}[R_{\mathcal{D}^{\text{te}}}(g) \mid g]]}_{(\text{A}) \text{ Expected evaluation noise}} + \underbrace{\text{Var}_g[\mathbb{E}[R_{\mathcal{D}^{\text{te}}}(g) \mid g]]}_{(\text{B}) \text{ Training instability}} . \quad (\text{B.2})$$

Term (B) equals $\text{Var}_g[\mathcal{R}^*(g)]$, which quantifies how much the true performance of the learned predictor varies across training sets and random seeds. Term (A) captures the finite-test-set evaluation noise.

By definition, δ_{HO} subtracts an estimator of the true risk from the finite-test-set score. Applying the law of total variance to δ_{HO} gives:

$$\text{Var}[\delta_{\text{HO}}] = \mathbb{E}_g[\text{Var}[\delta_{\text{HO}} \mid g]] + \text{Var}_g[\mathbb{E}[\delta_{\text{HO}} \mid g]] . \quad (\text{B.3})$$

Since $\widehat{R}^*(g)$ is unbiased conditional on g ,

$$\begin{aligned}\mathbb{E}[\delta_{\text{HO}} | g] &= \mathbb{E}\left[R_{\mathcal{D}^{\text{te}}}(g) - \widehat{R}^*(g) | g\right] \\ &= \mathcal{R}^*(g) - \mathcal{R}^*(g) = 0.\end{aligned}\tag{B.4}$$

Thus the conditional-mean term vanishes in the single-split case. Moreover, because $\widehat{R}^*(g)$ is constructed independently of \mathcal{D}^{te} conditional on g :

$$\begin{aligned}\text{Var}[\delta_{\text{HO}}] &= \mathbb{E}_g[\text{Var}[\delta_{\text{HO}} | g]] \\ &= \mathbb{E}_g[\text{Var}[R_{\mathcal{D}^{\text{te}}}(g) | g]] + \mathbb{E}_g[\text{Var}[\widehat{R}^*(g) | g]].\end{aligned}\tag{B.5}$$

Evaluation-noise approximation. Suppose that the expected evaluation noise of the oracle-score estimator $\widehat{R}^*(g)$ is negligible compared to that of the test set evaluation — in our experiments, $\widehat{R}^*(g)$ is computed on a large benchmarking set. We therefore treat its evaluation noise as negligible compared to the noise of the smaller held-out test set. Under this approximation,

$$\text{Var}[\delta_{\text{HO}}] \approx \mathbb{E}_g[\text{Var}[R_{\mathcal{D}^{\text{te}}}(g) | g]].\tag{B.6}$$

Thus $\text{Var}[\delta_{\text{HO}}]$ estimates the finite-test-sample evaluation noise, independently of the training-instability component.

Exact variance expansion for MCCV. For the MCCV procedure, let

$$g_k = F_\lambda(\mathcal{D}_{\eta_k}^{\text{tr}}, \xi_k), \quad \delta_k = R_{\mathcal{D}_{\eta_k}^{\text{te}}}(g_k) - \widehat{R}^*(g_k),$$

and define

$$\Delta_K = \frac{1}{K} \sum_{k=1}^K \delta_k = \underbrace{\widehat{R}_K}_{\text{CV Estimator}} - \underbrace{\frac{1}{K} \sum_{k=1}^K \widehat{R}^*(g_k)}_{\text{Estimated Oracle Score}}.\tag{B.7}$$

The variance decomposition used in the main text does not require conditioning on the learned predictors. It follows exactly from the unconditional covariance expansion. Under the MCCV split generator, the fold-level errors $\delta_1, \dots, \delta_K$ are exchangeable. Hence, for any k ,

$$\text{Var}(\delta_k) = \text{Var}(\delta_{\text{HO}}),\tag{B.8}$$

and for any distinct $i \neq j$ we define the unconditional benchmark-adjusted inter-fold covariance

$$\tau^{\text{te}} = \text{Cov}(\delta_i, \delta_j).\tag{B.9}$$

Then

$$\begin{aligned}\text{Var}(\Delta_K) &= \text{Var}\left[\frac{1}{K} \sum_{k=1}^K \delta_k\right] \\ &= \frac{1}{K^2} \sum_{k=1}^K \text{Var}(\delta_k) + \frac{1}{K^2} \sum_{\substack{i,j=1 \\ i \neq j}}^K \text{Cov}(\delta_i, \delta_j) \\ &= \frac{1}{K} \text{Var}(\delta_{\text{HO}}) + \frac{K-1}{K} \tau^{\text{te}}.\end{aligned}\tag{B.10}$$

This identity is exact. It includes all dependence induced by reusing the same finite study sample across MCCV splits: overlapping test sets, overlap between one fold's test set and another fold's training set, shared splitting randomness, and any residual dependence introduced by the benchmark correction.

C Estimating inter-fold covariance in cross-validation

This appendix derives the covariance quantities used throughout the paper. We first estimate the raw inter-fold covariance τ from fold scores, then apply the same ANOVA logic to benchmark-adjusted fold errors to estimate τ^{te} , the covariance quantity entering the test sample-gain formula.

C.1 Raw fold scores: estimating τ

Model. Fix an algorithm, dataset, and training-set size. For each independent seed $s = 1, \dots, S$, a K -split CV produces raw fold scores $E_{s,1}, \dots, E_{s,K}$, the seed-indexed version of the main-text fold score E_k . We model the scores as exchangeable within a seed, with

$$\text{Var}(E_{s,k}) = \sigma_{\text{HO}}^2, \quad \text{Cov}(E_{s,k}, E_{s,\ell}) = \tau \quad (k \neq \ell), \quad (\text{C.1})$$

where σ_{HO}^2 denotes the marginal variance of a single fold score — equivalently, under the matched test-set geometry used throughout this paper, the variance of a single held-out evaluation. Seeds are mutually independent. The parameter τ captures the irreducible covariance between fold scores that arises because all folds partially share the same training data [Nadeau and Bengio, 2003].

Sufficient statistics. For each seed s , define the fold mean and the within-seed sample variance:

$$\bar{E}_s = \frac{1}{K} \sum_{k=1}^K E_{s,k}, \quad V_s = \frac{1}{K-1} \sum_{k=1}^K (E_{s,k} - \bar{E}_s)^2. \quad (\text{C.2})$$

Under the model (C.1) (with no further distributional assumptions beyond finite fourth moments), their expectations are:

$$\mathbb{E}[V_s] = \sigma_{\text{HO}}^2 - \tau =: \sigma_{\text{HO,within}}^2, \quad (\text{C.3})$$

$$\mathbb{E}[\bar{E}_s] = \mu \quad (\text{some common mean}), \quad (\text{C.4})$$

$$\text{Var}(\bar{E}_s) = \frac{1}{K} \sigma_{\text{HO}}^2 + \frac{K-1}{K} \tau. \quad (\text{C.5})$$

The shorthand $\sigma_{\text{HO,within}}^2$ in (C.3) denotes the within-seed residual component of the raw fold-score variance. It is not a new population parameter: under the exchangeable model (C.1), the identity $\sigma_{\text{HO,within}}^2 = \sigma_{\text{HO}}^2 - \tau$ follows by expanding the within-seed sample variance. Equation (C.3) follows from expanding the within-seed variance and using the compound-symmetry covariance:

$$\mathbb{E}[V_s] = \frac{1}{K-1} \left[K \sigma_{\text{HO}}^2 - K \left(\frac{\sigma_{\text{HO}}^2}{K} + \frac{K-1}{K} \tau \right) \right] = \sigma_{\text{HO}}^2 - \tau.$$

ANOVA-type estimators. Averaging over seeds gives the “within” and “between” estimators:

$$\hat{W} = \frac{1}{S} \sum_{s=1}^S V_s, \quad \hat{B} = \frac{1}{S-1} \sum_{s=1}^S (\bar{E}_s - \bar{\bar{E}})^2, \quad \bar{\bar{E}} = \frac{1}{S} \sum_{s=1}^S \bar{E}_s. \quad (\text{C.6})$$

By (C.3) and (C.5),

$$\mathbb{E}[\hat{W}] = \sigma_{\text{HO}}^2 - \tau, \quad \mathbb{E}[\hat{B}] = \frac{\sigma_{\text{HO}}^2 + (K-1)\tau}{K}, \quad (\text{C.7})$$

so the method-of-moments (ANOVA) estimator of τ is

$$\hat{\tau} = \hat{B} - \frac{\hat{W}}{K}, \quad (\text{C.8})$$

with the companion estimator of σ_{HO}^2 ,

$$\hat{\sigma}_{\text{HO}|K}^2 := \hat{W} + \hat{\tau}, \quad (\text{C.9})$$

where the subscript “| K ” signals that this estimator is built *knowing* a K -fold CV run has been observed ($K \geq 2$); a complementary estimator $\hat{\sigma}_{\text{HO}|1}^2$ built from single-split replicates is introduced in Sec. D.1. Unbiasedness of $\hat{\tau}$ is immediate: $\mathbb{E}[\hat{\tau}] = \frac{\sigma_{\text{HO}}^2 + (K-1)\tau}{K} - \frac{\sigma_{\text{HO}}^2 - \tau}{K} = \tau$.

Remark. \hat{B} alone is already an unbiased estimator of $\text{Var}(\bar{E}_s)$, i.e. the variance of the K -split CV estimate. $\hat{\tau}$ refines this by subtracting the σ_{HO}^2/K contribution, isolating the floor $\lim_{K \rightarrow \infty} \text{Var}(\bar{E}_s) = \tau$.

Variance of $\hat{\tau}$. Since $\hat{\tau} = \hat{B} - \hat{W}/K$ and the two statistics are computed from the *same* fold scores, we need $\text{Var}(\hat{B})$, $\text{Var}(\hat{W})$, and $\text{Cov}(\hat{B}, \hat{W})$. Write $\theta_s = (\bar{E}_s, V_s)$ for the per-seed summary; these are i.i.d. across seeds.

Variance of \hat{B} . \hat{B} is the sample variance (ddof = 1) of the i.i.d. random variables $\bar{E}_1, \dots, \bar{E}_S$, each with variance $\gamma := \text{Var}(\bar{E}_s) = (\sigma_{\text{HO}}^2 + (K-1)\tau)/K$ and fourth central moment $\mu_4 := \mathbb{E}[(\bar{E}_s - \mu)^4]$.

Write $(S-1)\hat{B} = \sum_s (\bar{E}_s - \mu)^2 - S(\bar{\bar{E}} - \mu)^2$. The three needed variances and covariance are:

$$\text{Var}\left(\sum_s (\bar{E}_s - \mu)^2\right) = S(\mu_4 - \gamma^2), \quad (\text{C.10})$$

$$\text{Var}(S(\bar{\bar{E}} - \mu)^2) = \frac{\mu_4}{S} + \frac{2S-3}{S} \gamma^2, \quad (\text{C.11})$$

$$\text{Cov}\left(\sum_s (\bar{E}_s - \mu)^2, S(\bar{\bar{E}} - \mu)^2\right) = \mu_4 - \gamma^2, \quad (\text{C.12})$$

all obtained by expanding in terms of $\mathbb{E}[(\bar{E}_s - \mu)^4] = \mu_4$ and $\mathbb{E}[(\bar{E}_s - \mu)^2] = \gamma$ and using independence across seeds. In particular, $\mathbb{E}[(\sum_s (\bar{E}_s - \mu)^2)^4] = S\mu_4 + 3S(S-1)\gamma^2$ (only the diagonal and pairwise-square terms survive). Combining via $\text{Var}((S-1)\hat{B}) = \text{Var}(\sum (\bar{E}_s - \mu)^2) + \text{Var}(S(\bar{\bar{E}} - \mu)^2) - 2 \text{Cov}$ and simplifying:

$$\text{Var}(\hat{B}) = \frac{1}{S} \left(\mu_4 - \frac{S-3}{S-1} \gamma^2 \right). \quad (\text{C.13})$$

Under Gaussian fold scores, \bar{E}_s is Gaussian so $\mu_4 = 3\gamma^2$ (kurtosis $\kappa = 3$), and this reduces to $\text{Var}(\hat{B}) = 2\gamma^2/(S-1)$.

Variance of \hat{W} . $\hat{W} = \frac{1}{S} \sum_s V_s$ is a sample mean of i.i.d. terms with mean $\sigma_{\text{HO}}^2 - \tau$ and variance $\text{Var}(V_s)$. Hence:

$$\text{Var}(\hat{W}) = \frac{\text{Var}(V_s)}{S}. \quad (\text{C.14})$$

Under joint normality of $(E_{s,1}, \dots, E_{s,K})$ with the compound-symmetry covariance $\Sigma = (\sigma_{\text{HO}}^2 - \tau)I_K + \tau\mathbf{1}\mathbf{1}^\top$, the quadratic form $(K-1)V_s = \mathbf{E}_s^\top M \mathbf{E}_s$ (where $M = I_K - \frac{1}{K}\mathbf{1}\mathbf{1}^\top$) satisfies $(K-1)V_s/(\sigma_{\text{HO}}^2 - \tau) \sim \chi_{K-1}^2$, giving $\text{Var}(V_s) = 2(\sigma_{\text{HO}}^2 - \tau)^2/(K-1)$, so

$$\text{Var}(\hat{W}) = \frac{2(\sigma_{\text{HO}}^2 - \tau)^2}{S(K-1)}. \quad (\text{C.15})$$

Covariance of \hat{B} and \hat{W} . Under normality, \bar{E}_s and V_s are independent within each seed (a consequence of Fisher–Cochran: the projection onto $\text{span}(\mathbf{1})$ is orthogonal to the range of M , and since $\mathbf{1}$ is an eigenvector of Σ , the two resulting Gaussian components are uncorrelated and hence independent). Since \hat{B} depends only on $(\bar{E}_1, \dots, \bar{E}_S)$ and \hat{W} only on (V_1, \dots, V_S) , they are independent, and $\text{Cov}(\hat{B}, \hat{W}) = 0$.

Combining. Under normality,

$$\boxed{\text{Var}(\hat{\tau}) = \text{Var}(\hat{B}) + \frac{1}{K^2} \text{Var}(\hat{W}) = \frac{2(\sigma_{\text{HO}}^2 + (K-1)\tau)^2}{K^2(S-1)} + \frac{2(\sigma_{\text{HO}}^2 - \tau)^2}{S K^2(K-1)}}. \quad (\text{C.16})$$

Interpretation. As K grows, the second term (from \hat{W}) vanishes as $O(K^{-3})$, while the first (from \hat{B}) dominates and converges to $2\tau^2/(S-1)$. The precision of $\hat{\tau}$ is then ultimately limited by how many independent seeds S we observe.

Plug-in and bootstrap. In practice, we replace $(\sigma_{\text{HO}}^2, \tau, \mu_4)$ by their sample counterparts $(\hat{\sigma}_{\text{HO}|K}^2, \hat{\tau}, \hat{\mu}_4)$ to evaluate (C.16). Because the Gaussian kurtosis assumption ($\kappa = 3$) may not hold, our implementation supplements the plug-in formula with a non-parametric bootstrap over seeds: resample $(\bar{E}_s, V_s)_{s=1}^S$ with replacement 100 times, recompute $\hat{\tau}$ for each replicate, and report percentile confidence intervals. This is valid because the seed-level summaries are i.i.d., making the ordinary bootstrap consistent for their functionals.

Relation to the Bengio–Grandvalet impossibility. Bengio and Grandvalet [2004] show that no unbiased estimator of $\text{Var}(\bar{E}_K)$ can be constructed from the scores of a single K -fold CV run. Our estimator does not contradict this result: it requires $S \geq 2$ *independent replications* of the entire K -fold procedure (each on a fresh random seed), making $\bar{E}_1, \dots, \bar{E}_S$ an i.i.d. sample whose variance is trivially estimable. The Bengio–Grandvalet impossibility applies to the single-run regime ($S = 1$), which is the common practical setting but not ours.

The raw covariance τ is useful for understanding how fold scores move together, but it still contains training-side drift shared by the fold predictors. For estimating test sample gains, we therefore apply the same estimation strategy to benchmark-adjusted fold errors.

C.2 Benchmark-adjusted fold errors: estimating τ^{te}

From raw fold scores to benchmark-adjusted deltas. The raw-score inter-fold covariance τ of Sec. C.1 is dominated by the training-side randomness shared by the K fold-specific training problems: within one seed, the K predictors are learned from overlapping study data and their fold scores move together when the seed-level training process drifts. In practice, we care about how much each fold score *disagrees with a benchmark*, not about the raw fold similarity. Define the benchmark-adjusted fold score

$$\delta_{s,k} = E_{s,k} - \widehat{R}_{s,k}^*(g_{s,k}), \quad (\text{C.17})$$

where $E_{s,k} = R_{\mathcal{D}_{s,k}^{\text{te}}}(g_{s,k})$ is the raw test score of the fold-specific predictor $g_{s,k} = F_\lambda(\mathcal{D}_{s,k}^{\text{tr}}, \xi_{s,k})$, and $\widehat{R}_s^*(g_{s,k})$ is its benchmark-set estimate, computed independently of the fold test set. The inter-fold covariance on δ ,

$$\tau^{\text{te}} = \text{Cov}(\delta_{s,k}, \delta_{s,\ell}) \quad (k \neq \ell), \quad (\text{C.18})$$

is the fold covariance that remains *after* the benchmark has cancelled the training-side drift.

By the law of total covariance, this unconditional covariance can be written as:

$$\tau^{\text{te}} = \text{Cov}(\delta_{s,k}, \delta_{s,\ell}) = \mathbb{E}_G[\text{Cov}(\delta_{s,k}, \delta_{s,\ell} \mid G)] + \text{Cov}_G(\mathbb{E}[\delta_{s,k} \mid G], \mathbb{E}[\delta_{s,\ell} \mid G]). \quad (\text{C.19})$$

The second term need not vanish in MCCV, because observations held out in one split may appear in the training sets of other split predictors. Our estimator targets the unconditional covariance, which is the quantity entering the exact variance formula for Δ_K (see (15)).

Model. Fix an algorithm, dataset, training-set size, and benchmark set. For each independent seed $s = 1, \dots, S$, the K -split CV and the benchmark evaluation together produce $\delta_{s,1}, \dots, \delta_{s,K}$. We model these as exchangeable within a seed, with

$$\text{Var}(\delta_{s,k}) = \sigma^{2,\text{te}}, \quad \text{Cov}(\delta_{s,k}, \delta_{s,\ell}) = \tau^{\text{te}} \quad (k \neq \ell), \quad (\text{C.20})$$

and seeds mutually independent. Here $\sigma^{2,\text{te}}$ is the bench-adjusted analogue of σ_{HO}^2 : the marginal variance of a single δ fold score, equivalently the variance of a single bench-adjusted held-out evaluation under the matched test-set geometry used throughout this paper. Exchangeability is therefore an explicit working model for these benchmark-adjusted fold scores; it is appropriate when the split-generation and benchmark-evaluation procedures are symmetric in the fold index k .

Sufficient statistics. Mirroring (C.2), define the per-seed delta mean and within-seed delta variance:

$$\bar{\delta}_s = \frac{1}{K} \sum_{k=1}^K \delta_{s,k}, \quad V_s^\delta = \frac{1}{K-1} \sum_{k=1}^K (\delta_{s,k} - \bar{\delta}_s)^2. \quad (\text{C.21})$$

Under (C.20),

$$\mathbb{E}[V_s^\delta] = \sigma^{2,\text{te}} - \tau^{\text{te}} =: \sigma_{\text{within}}^{2,\text{te}}, \quad (\text{C.22})$$

$$\text{Var}(\bar{\delta}_s) = \frac{\sigma^{2,\text{te}} + (K-1)\tau^{\text{te}}}{K}. \quad (\text{C.23})$$

The shorthand $\sigma_{\text{within}}^{2,\text{te}} := \sigma^{2,\text{te}} - \tau^{\text{te}}$ is the bench-adjusted analogue of $\sigma_{\text{HO,within}}^2$ from (C.3): it is the within-seed residual component of the benchmark-adjusted fold-score variance.

ANOVA-type estimators. Averaging across seeds:

$$\hat{W}_\delta = \frac{1}{S} \sum_{s=1}^S V_s^\delta, \quad \hat{B}_\delta = \frac{1}{S-1} \sum_{s=1}^S (\bar{\delta}_s - \bar{\delta})^2, \quad \bar{\delta} = \frac{1}{S} \sum_{s=1}^S \bar{\delta}_s, \quad (\text{C.24})$$

with expectations

$$\mathbb{E}[\hat{W}_\delta] = \sigma^{2,\text{te}} - \tau^{\text{te}}, \quad \mathbb{E}[\hat{B}_\delta] = \frac{\sigma^{2,\text{te}} + (K-1)\tau^{\text{te}}}{K}, \quad (\text{C.25})$$

yielding the method-of-moments estimator

$$\hat{\tau}^{\text{te}} = \hat{B}_\delta - \frac{\hat{W}_\delta}{K}, \quad (\text{C.26})$$

and companion estimator of $\sigma^{2,\text{te}}$,

$$\hat{\sigma}_{|K}^{2,\text{te}} := \hat{W}_\delta + \hat{\tau}^{\text{te}}, \quad (\text{C.27})$$

the bench-adjusted analogue of (C.9), again subscripted “ $|K$ ” to indicate that it is built *knowing* a K -fold CV run has been observed ($K \geq 2$). Unbiasedness follows identically to Sec. C.1:

$$\mathbb{E}[\hat{\tau}^{\text{te}}] = (\sigma^{2,\text{te}} + (K-1)\tau^{\text{te}})/K - (\sigma^{2,\text{te}} - \tau^{\text{te}})/K = \tau^{\text{te}}. \quad (\text{C.28})$$

In practice, (C.26) is computed by applying the raw estimator (C.8) to the delta column $\delta_{s,k}$ rather than to the raw fold-score column $E_{s,k}$; no new estimator machinery is needed.

Remark. \hat{B}_δ alone is unbiased for $\text{Var}(\bar{\delta}_s)$, the variance of the benchmark-adjusted K -split CV estimate. $\hat{\tau}^{\text{te}}$ then isolates the irreducible $K \rightarrow \infty$ floor on that variance.

Variance of $\hat{\tau}^{\text{te}}$. The derivation in Sec. C.1 relied only on compound symmetry within seeds and independence across seeds, both inherited by (C.20). All steps therefore transfer verbatim under the substitutions $(\sigma_{\text{HO}}^2, \tau) \mapsto (\sigma^{2,\text{te}}, \tau^{\text{te}})$, $(V_s, \bar{E}_s) \mapsto (V_s^\delta, \bar{\delta}_s)$. Writing $\gamma_\delta := \text{Var}(\bar{\delta}_s) = (\sigma^{2,\text{te}} + (K-1)\tau^{\text{te}})/K$ and $\mu_4^\delta := \mathbb{E}[(\bar{\delta}_s - \mu_\delta)^4]$, the analogue of (C.13) is

$$\text{Var}(\hat{B}_\delta) = \frac{1}{S} \left(\mu_4^\delta - \frac{S-3}{S-1} \gamma_\delta^2 \right), \quad (\text{C.29})$$

and, under joint Gaussianity of $(\delta_{s,1}, \dots, \delta_{s,K})$ with compound-symmetry covariance $\Sigma_\delta = (\sigma^{2,\text{te}} - \tau^{\text{te}})I_K + \tau^{\text{te}}\mathbf{1}\mathbf{1}^\top$, the quadratic form $(K-1)V_s^\delta$ is $(\sigma^{2,\text{te}} - \tau^{\text{te}})\chi_{K-1}^2$, giving

$$\text{Var}(\hat{W}_\delta) = \frac{2(\sigma^{2,\text{te}} - \tau^{\text{te}})^2}{S(K-1)}. \quad (\text{C.30})$$

Gaussianity together with compound symmetry implies $\bar{\delta}_s \perp V_s^\delta$ within each seed (Fisher–Cochran, exactly as in Sec. C.1), so $\text{Cov}(\hat{B}_\delta, \hat{W}_\delta) = 0$, and combining:

$$\text{Var}(\hat{\tau}^{\text{te}}) = \text{Var}(\hat{B}_\delta) + \frac{1}{K^2} \text{Var}(\hat{W}_\delta) = \frac{2(\sigma^{2,\text{te}} + (K-1)\tau^{\text{te}})^2}{K^2(S-1)} + \frac{2(\sigma^{2,\text{te}} - \tau^{\text{te}})^2}{S K^2(K-1)}. \quad (\text{C.31})$$

Interpretation. The K -scaling parallels the raw case: the \hat{W}_δ contribution vanishes as $O(K^{-3})$ while $\text{Var}(\hat{B}_\delta) \rightarrow 2(\tau^{\text{te}})^2/(S-1)$, so precision is again ultimately seed-limited. Crucially, the asymptotic floor $2(\tau^{\text{te}})^2/(S-1)$ is quadratic in τ^{te} , which is typically one to three orders of magnitude smaller than τ due to benchmark cancellation. The same seed budget therefore yields confidence intervals on $\hat{\tau}^{\text{te}}$ that are orders of magnitude tighter than on $\hat{\tau}$.

Plug-in and bootstrap. We evaluate (C.31) with the sample counterparts $(\hat{\sigma}_{|K}^{2,\text{te}}, \hat{\tau}^{\text{te}}, \hat{\mu}_4^\delta)$, and supplement it with a non-parametric bootstrap over seeds: resample $(\bar{\delta}_s, V_s^\delta)_{s=1}^S$ with replacement 100 times, recompute $\hat{\tau}^{\text{te}}$ per replicate via (C.26), and report percentile confidence intervals. This is valid for the same reason as in the raw case: the seed-level summaries $(\bar{\delta}_s, V_s^\delta)$ are i.i.d., making the ordinary bootstrap consistent for their functionals. No separate code path is required — our implementation calls the raw $\hat{\tau}$ routine with $\delta_{s,k}$ as the input column.

Relation to the Bengio–Grandvalet impossibility. As with $\hat{\tau}$, the consistency of $\hat{\tau}^{\text{te}}$ is not in conflict with the impossibility result of Bengio and Grandvalet [2004]: the latter applies to single-run ($S = 1$) variance estimation, whereas our setting requires $S \geq 2$ independent seed-level replications of the whole (K -fold + benchmark) procedure, making $\bar{\delta}_1, \dots, \bar{\delta}_S$ an i.i.d. sample whose variance is trivially estimable.

D Estimating and anticipating sample gains

This section gathers the operational tools used to estimate or anticipate test sample gains. We first derive a benchmark-aware estimator based on $\hat{\tau}^{\text{te}}$. We then give a non-benchmark proxy that preserves the same variance-ratio structure when benchmark scores are unavailable. Finally, we introduce a study-only redundancy statistic for deciding, after only a few splits of a single CV run, whether further repetitions are likely to pay off.

D.1 Benchmark-aware estimation of sample gain G_K^{test}

Operational question. A practitioner who has budgeted for S independent repetitions must decide whether to spend each repetition on a single-holdout evaluation or on a full K -split CV evaluation at the same training size n_{tr} and fold test size n_{te} . For repetition s , let $\delta_{\text{HO}}^{(s)}$ be the single-holdout version of the main-text estimation error δ_{HO} from (11), and let

$$\Delta_K^{(s)} := \frac{1}{K} \sum_{k=1}^K \delta_{s,k} \quad (\text{D.1})$$

be the seed-level version of the main-text K -split estimation error Δ_K , with $\delta_{s,k}$ defined as in (C.17). Thus

$$V_1^\delta(n_{\text{te}}) = \text{Var}\left(\delta_{\text{HO}}^{(s)}\right), \quad V_K^\delta(n_{\text{te}}) = \text{Var}\left(\Delta_K^{(s)}\right). \quad (\text{D.2})$$

The exact main-text sample gain $G_K^{\text{test}}(F_\lambda, n_{\text{tr}})$ is defined in (17) through the variance-equivalent test size N_K^{equiv} . The covariance estimators of Sec. C.2 estimate the same sample-gain notation through the local variance-ratio approximation introduced immediately after (17):

$$G_K^{\text{test}}(F_\lambda, n_{\text{tr}}) \approx \frac{V_1^\delta(n_{\text{te}})}{V_K^\delta(n_{\text{te}})} = \frac{\text{Var}\left(\delta_{\text{HO}}^{(s)}\right)}{\text{Var}\left(\Delta_K^{(s)}\right)}. \quad (\text{D.3})$$

The approximation sign is the same $1/m$ test-size scaling approximation used in the main text: no separate sample-gain symbol is introduced in this appendix. Values of $G_K^{\text{test}}(F_\lambda, n_{\text{tr}})$ close to K mean K -split CV is as informative as K independent holdout evaluations; values close to 1 mean the folds are effectively redundant and CV does not reduce variance below a single holdout.

Decomposition in terms of τ^{te} and $\sigma^{2,\text{te}}$. By (C.23), the CV-estimation-error variance is

$$V_K^\delta(n_{\text{te}}) = \text{Var}(\Delta_K^{(s)}) = \text{Var}(\bar{\delta}_s) = \frac{\sigma^{2,\text{te}} + (K-1)\tau^{\text{te}}}{K}, \quad (\text{D.4})$$

which is the population quantity estimated directly by \hat{B}_δ . Under the matched test-set geometry used throughout this paper, the single-holdout variance equals the marginal δ -score variance introduced in Sec. C.2:

$$V_1^\delta(n_{\text{te}}) = \text{Var}\left(\delta_{\text{HO}}^{(s)}\right) = \text{Var}(\delta_{s,k}) = \sigma^{2,\text{te}}. \quad (\text{D.5})$$

Substituting into (D.3) gives

$$\boxed{G_K^{\text{test}}(F_\lambda, n_{\text{tr}}) \approx \frac{K \sigma^{2,\text{te}}}{\sigma^{2,\text{te}} + (K-1)\tau^{\text{te}}} = \frac{\sigma^{2,\text{te}}}{\text{Var}(\Delta_K^{(s)})}}. \quad (\text{D.6})$$

The first form expresses the test sample gain using the two ANOVA-aligned estimands of Sec. C.2; the second form makes clear that the gain is the ratio of the single-HO and CV-estimation-error variances of the benchmark-adjusted δ score.

Remark (idealised gain). If the benchmark is geometrically matched to training so that $\tau^{\text{te}} = 0$, (D.6) recovers the textbook $G_K^{\text{test}}(F_\lambda, n_{\text{tr}}) \approx K$. Every departure from K in an observed $\widehat{G}_K^{\text{test}}(F_\lambda, n_{\text{tr}})$ therefore reflects residual fold correlation $\tau^{\text{te}} > 0$.

Intraclass-correlation form. Under the matched test-set geometry of (D.6), we can rewrite the gain approximation in intraclass-correlation (ICC) form:

$$G_K^{\text{test}}(F_\lambda, n_{\text{tr}}) \approx \frac{K}{1 + (K-1)\rho_\delta}, \quad \rho_\delta := \frac{\tau^{\text{te}}}{\sigma^{2,\text{te}}}. \quad (\text{D.7})$$

The ratio $\rho_\delta \in [0, 1]$ is the intraclass correlation of the fold δ -scores; it is scale-free, requires no external single-holdout seeds, and is directly estimable from the ANOVA decomposition of a single K -split experiment. This gives a compact decision rule:

$$\rho_\delta \ll \frac{1}{K-1} \Rightarrow G_K^{\text{test}}(F_\lambda, n_{\text{tr}}) \approx K; \quad \rho_\delta \rightarrow 1 \Rightarrow G_K^{\text{test}}(F_\lambda, n_{\text{tr}}) \approx 1 \text{ (CV is redundant)}. \quad (\text{D.8})$$

Figure D.1 illustrates this relationship empirically: the observed gains decrease sharply as the estimated fold-error correlation $\widehat{\rho}_\delta$ increases, in agreement with the ICC approximation.

Figure D.1 illustrates the empirical content of (D.8). When the estimated fold-error correlation is small, the repeated split evaluations retain complementary information and the observed sample gain can be large. Conversely, as $\widehat{\rho}_\delta$ increases, folds become more redundant and the attainable gain decreases. The monotone trend follows the ICC curve closely enough to make $\widehat{\rho}_\delta$ a useful diagnostic for understanding why a given K -split CV run does or does not approach the ideal gain K .

Plug-in estimator. Replacing each quantity in (D.6) by its sample counterpart gives the estimator used for the reported test sample gains:

$$\widehat{G}_K^{\text{test}}(F_\lambda, n_{\text{tr}}) = \frac{\widehat{V}_1^\delta(n_{\text{te}})}{\widehat{V}_K^\delta(n_{\text{te}})} = \frac{\widehat{\sigma}_{|1}^{2,\text{te}}}{\widehat{B}_\delta} = \frac{K \widehat{\sigma}_{|1}^{2,\text{te}}}{\widehat{\sigma}_{|K}^{2,\text{te}} + (K-1)\widehat{\tau}^{\text{te}}} \quad (\text{D.9})$$

Here $\widehat{V}_K^\delta(n_{\text{te}}) = \widehat{B}_\delta$ estimates $V_K^\delta(n_{\text{te}})$, while $\widehat{V}_1^\delta(n_{\text{te}}) = \widehat{\sigma}_{|1}^{2,\text{te}}$ is the bench-adjusted across-seed sample variance of the single-holdout estimation errors $(\delta_{\text{HO}}^{(s)})_{s=1}^{S_{\text{HO}}}$:

$$\widehat{\sigma}_{|1}^{2,\text{te}} := \frac{1}{S_{\text{HO}} - 1} \sum_{s=1}^{S_{\text{HO}}} (\delta_{\text{HO}}^{(s)} - \bar{\delta}_{\text{HO}})^2. \quad (\text{D.10})$$

The subscript “| 1” signals that this estimator is built *knowing* a set of single-split runs has been observed (the degenerate $K = 1$ case), and mirrors the “| K ” convention introduced for $\widehat{\sigma}_{|K}^{2,\text{te}}$. The last equality in (D.9) follows from $\widehat{\sigma}_{|K}^{2,\text{te}} + (K-1)\widehat{\tau}^{\text{te}} = K\widehat{B}_\delta$ (by (C.27) and (C.26)) and shows that every seed-level quantity contributing to $\widehat{G}_K^{\text{test}}(F_\lambda, n_{\text{tr}})$ is either a sample variance or a linear combination of sample variances — no iterative solver or bespoke numerical routine is required.

Remark (choice of the single-holdout variance estimator). The main-paper quantity $G_K^{\text{test}}(F_\lambda, n_{\text{tr}})$ is based on $V_1^\delta(n_{\text{te}})$, so the numerator of (D.9) must target the marginal single-holdout benchmark-adjusted variance $\sigma^{2,\text{te}}$. This is why the plug-in estimator uses $\widehat{\sigma}_{|1}^{2,\text{te}}$. A within-seed variant,

$$\widehat{\sigma}_{\text{within}}^{2,\text{te}} := (\text{within-seed variance of benchmark-adjusted fold scores, averaged across seeds}), \quad (\text{D.11})$$

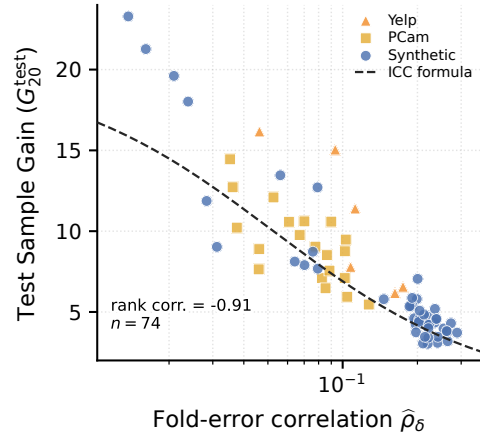


Figure D.1: Estimated fold-error correlation $\widehat{\rho}_\delta$ versus observed G_{20}^{test} . The dashed curve is the ICC approximation $K/(1 + (K-1)\widehat{\rho}_\delta)$.

estimates the distinct population quantity $\sigma_{\text{within}}^{2,\text{te}} = \sigma^{2,\text{te}} - \tau^{\text{te}}$ introduced in (C.22). It should therefore be treated as a within-seed diagnostic, not as the numerator of the main-paper sample gain, unless a separate within-seed gain is explicitly defined.

Uncertainty. Because $\widehat{G}_K^{\text{test}}(F_\lambda, n_{\text{tr}})$ is a ratio of two sample variances, an analytic variance expression requires either a delta-method expansion with fourth-moment terms or an independence assumption on the seed populations behind the numerator and denominator. Under independence of the two seed populations and a log-delta approximation,

$$\text{Var}\left(\log \widehat{G}_K^{\text{test}}(F_\lambda, n_{\text{tr}})\right) \approx \frac{\text{Var}(\hat{\sigma}_{|1}^{2,\text{te}})}{(\sigma^{2,\text{te}})^2} + \frac{\text{Var}(\hat{B}_\delta)}{\gamma_\delta^2}, \quad (\text{D.12})$$

with $\text{Var}(\hat{B}_\delta)$ from (C.29) and the numerator analogue having the same sample-variance form. In practice we prefer a non-parametric bootstrap because it sidesteps the fourth-moment and independence assumptions. We resample seeds with replacement $B = 1000$ times (independently for the CV seed set and for the HO seed set when they differ), recompute $(\hat{B}_\delta, \hat{\sigma}_{|1}^{2,\text{te}})$ and the ratio (D.9) on each replicate, and report percentile confidence intervals for $\widehat{G}_K^{\text{test}}(F_\lambda, n_{\text{tr}})$. Since $\widehat{G}_K^{\text{test}}$ is a smooth functional of i.i.d. seed summaries, the ordinary bootstrap is consistent.

Interpretation. Combining the results of Sec. C.2 with (D.9), we obtain confidence intervals on $\widehat{G}_K^{\text{test}}(F_\lambda, n_{\text{tr}})$ whose width is controlled jointly by S (number of CV seeds) and S_{HO} (number of single-holdout seeds). As K grows with S fixed, both the variance-ratio approximation (D.6) and its intraclass-correlation form (D.7) approach the asymptotic bound

$$G_K^{\text{test}}(F_\lambda, n_{\text{tr}}) \xrightarrow{K \rightarrow \infty} \frac{\sigma^{2,\text{te}}}{\tau^{\text{te}}}, \quad (\text{D.13})$$

so the irreducible ceiling on the test sample gain is dictated entirely by the ratio of the single-holdout variance to the residual fold covariance τ^{te} . When τ^{te} has been estimated tightly (as it typically is when $\tau^{\text{te}} \ll \tau$, cf. Sec. C.2), this ceiling is likewise tight, and the practitioner can commit to CV or single holdout with a quantified rather than heuristic rationale.

This is the target quantity in our experiments, but it relies on benchmark-adjusted scores. The next subsection asks what can still be inferred when no large benchmarking set is available.

D.2 A non-benchmark proxy for sample gain G_K^{test}

Motivation. The plug-in estimator (D.9) uses benchmark-adjusted quantities:

$$\widehat{G}_K^{\text{test}}(F_\lambda, n_{\text{tr}}) = \frac{K \hat{\sigma}_{|1}^{2,\text{te}}}{\hat{\sigma}_{|K}^{2,\text{te}} + (K-1)\hat{\tau}^{\text{te}}}. \quad (\text{D.14})$$

This is the target quantity in our experiments, but it cannot be used when benchmark scores are unavailable. We therefore build a *rowwise non-benchmark proxy*: for each fixed algorithm, dataset, and training-set size, the proxy is computed only from the raw-score quantities of that same setup.

Recall from Sec. C.1 that

$$\hat{\sigma}_{\text{HO}|K}^2 = \hat{W} + \hat{\tau}, \quad \hat{\sigma}_{\text{HO},\text{within}}^2 = \hat{W}, \quad (\text{D.15})$$

where $\hat{\sigma}_{\text{HO}|K}^2$ estimates the marginal raw held-out variance observed through a K -split experiment, while $\hat{\sigma}_{\text{HO},\text{within}}^2$ estimates the within-seed residual variance. Let $\hat{\sigma}_{\text{HO}|1}^2$ denote the corresponding raw single-holdout variance estimate.

Best empirical proxy. The best-performing non-benchmark formula in our rowwise search keeps the same variance-ratio structure as (D.9), but replaces the unavailable benchmark-adjusted terms by

raw-score surrogates:

$$\tilde{\sigma}_{\text{num}}^2 := \left(\hat{\sigma}_{\text{HO}|K}^2 \hat{\sigma}_{\text{HO,within}}^2 \right)^{1/2}, \quad (\text{D.16})$$

$$\tilde{\sigma}_{\text{den}}^2 := \frac{1}{4} \hat{\sigma}_{\text{HO}|1}^2 + \frac{3}{4} \hat{\sigma}_{\text{HO,within}}^2, \quad (\text{D.17})$$

$$\tilde{\tau}_{\text{NB}}^{\text{te}} := 0.60 \hat{\tau} \frac{\hat{\sigma}_{\text{HO,within}}^2}{\hat{\sigma}_{\text{HO}|K}^2}. \quad (\text{D.18})$$

The resulting sample-gain proxy is

$$\tilde{G}_{K,\text{NB}}^{\text{rtest}}(F_\lambda, n_{\text{tr}}) = \frac{K \left(\hat{\sigma}_{\text{HO}|K}^2 \hat{\sigma}_{\text{HO,within}}^2 \right)^{1/2}}{\frac{1}{4} \hat{\sigma}_{\text{HO}|1}^2 + \frac{3}{4} \hat{\sigma}_{\text{HO,within}}^2 + (K-1) 0.60 \hat{\tau} \frac{\hat{\sigma}_{\text{HO,within}}^2}{\hat{\sigma}_{\text{HO}|K}^2}}. \quad (\text{D.19})$$

Figure D.2 shows that this non-benchmark proxy captures a substantial part of the ordering of observed sample gains, although it should be interpreted as a calibrated diagnostic rather than an unbiased estimator. The proxy is not intended to be an unbiased estimator of the exact sample gain, but it captures a substantial part of the ordering of the observed gains while using only raw quantities computed from the same algorithm–dataset–training-size setup. It should therefore be read as a practical diagnostic: large predicted values indicate settings where multi-split CV is likely to be valuable, whereas small predicted values suggest more redundant repetitions.

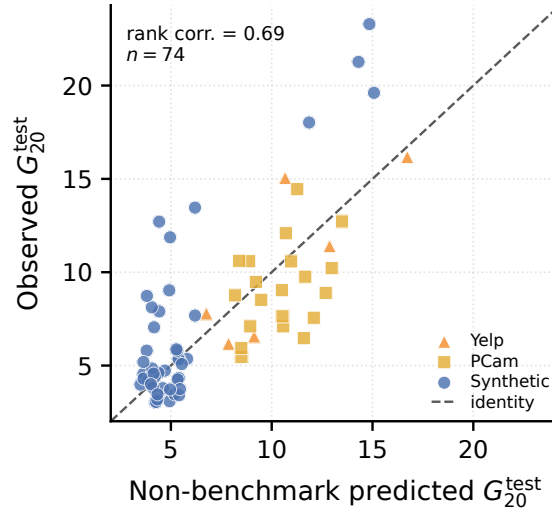


Figure D.2: Observed sample gain versus the non-benchmark rowwise proxy defined in (D.19).

Interpretation. Equation (D.19) mirrors the benchmark-based test sample-gain formula:

$$\text{sample gain} = \frac{K \times \text{single-HO variance}}{\text{CV marginal variance} + (K-1) \times \text{inter-fold covariance}}.$$

The numerator $\tilde{\sigma}_{\text{num}}^2$ is a geometric mean between the raw marginal variance $\hat{\sigma}_{\text{HO}|K}^2$ and the within-seed residual variance $\hat{\sigma}_{\text{HO,within}}^2$. This is useful because the benchmark-adjusted single-HO variance is typically smaller than the full raw marginal variance, but larger than the purely within-seed residual variance.

The denominator variance term $\tilde{\sigma}_{\text{den}}^2$ puts most of its weight on $\hat{\sigma}_{\text{HO,within}}^2$, because benchmarking is intended to remove a large part of the training-side drift. The remaining 1/4 contribution from $\hat{\sigma}_{\text{HO}|1}^2$ allows the proxy to retain some marginal single-holdout variability.

Finally, the raw covariance $\hat{\tau}$ is not used directly as a proxy for τ^{te} , because $\hat{\tau}$ includes training-side covariance that the benchmark largely cancels. The factor $\frac{\hat{\sigma}_{\text{Ho},\text{within}}^2}{\hat{\sigma}_{\text{Ho}|K}^2}$ shrinks $\hat{\tau}$ according to the fraction of raw variance that remains after conditioning on the trained model. When raw fold variation is dominated by shared training drift, this ratio is small, and the proxy strongly reduces the effective covariance. When raw fold variation is mostly evaluation-side noise, the ratio is closer to one, and less shrinkage is applied. The numerical factor 0.60 is an empirical calibration constant selected by the rowwise proxy search.

Remark. The quantity $\tilde{G}_{K,\text{NB}}^{\text{test}}(F_\lambda, n_{\text{tr}})$ is not claimed to be an unbiased estimator of $G_K^{\text{test}}(F_\lambda, n_{\text{tr}})$. It is a calibrated non-benchmark proxy: it preserves the structure of the theoretical sample-gain formula, uses only raw quantities computed on the same setup, and avoids using $\hat{\tau}^{\text{te}}$, $\hat{\sigma}_{|K}^{2,\text{te}}$, $\hat{\sigma}_{|1}^{2,\text{te}}$, or any benchmark score at prediction time.

The rowwise proxy estimates the magnitude of the gain from summary statistics. A complementary practical question is whether one can stop a CV run early. The next subsection addresses this by using only the first few split-specific predictors of a single run.

D.3 Study-only redundancy for early-stopping cross-validation

Operational goal. The exact test sample gain in (17) requires an outer set and a large benchmarking set. Practitioners usually do not have these quantities when deciding whether to spend more compute on additional splits. The goal of this section is therefore different: after only a few splits of a single CV run, can one decide whether continuing CV is likely to pay off?

The statistic below is computed from the study set only. It uses neither the outer set nor the benchmarking set, and it does not average over several experimental seeds. In practice, after observing the first k splits of one CV run, with k as small as 2 or 3, one computes the statistic on these already-trained predictors. It should be interpreted as a triage rule rather than an unbiased estimator of $G_K^{\text{test}}(F_\lambda, n_{\text{tr}})$: high redundancy suggests stopping early, whereas low redundancy indicates that larger gains remain plausible.

Single-run redundancy score. Consider one partial CV run, indexed by s , after k splits. For split $a \in \{1, \dots, k\}$, keep the main-paper notation

$$g_{a,s} = F_\lambda(\mathcal{D}_{\eta_{a,s}}^{\text{tr}}, \xi_{a,s}), \quad \mathcal{D}_{a,s}^{\text{te}} = \mathcal{D}_{\eta_{a,s}}^{\text{te}}.$$

For two splits $a < b$, let

$$I_{ab,s} = \mathcal{D}_{a,s}^{\text{te}} \cap \mathcal{D}_{b,s}^{\text{te}}$$

be the study observations held out in both splits. For $i \in I_{ab,s}$, define the out-of-fold loss

$$e_{a,s,i} = \ell(g_{a,s}(x_i), y_i),$$

which is the squared error in the synthetic regression experiments. We compute the pair-averaged loss covariance and loss variance

$$\hat{C}_{e,k,s}^{\text{study}} = \binom{k}{2}^{-1} \sum_{a < b} \widehat{\text{Cov}}_{i \in I_{ab,s}}(e_{a,s,i}, e_{b,s,i}), \quad (\text{D.20})$$

$$\hat{V}_{e,k,s}^{\text{study}} = \binom{k}{2}^{-1} \sum_{a < b} \frac{1}{2} \left(\widehat{\text{Var}}_{i \in I_{ab,s}}(e_{a,s,i}) + \widehat{\text{Var}}_{i \in I_{ab,s}}(e_{b,s,i}) \right), \quad (\text{D.21})$$

and their ratio

$$\hat{\rho}_{e,k,s}^{\text{study}} = \frac{\hat{C}_{e,k,s}^{\text{study}}}{\hat{V}_{e,k,s}^{\text{study}}}. \quad (\text{D.22})$$

This quantity acts like a study-only error correlation: it is large when different fold predictors tend to be wrong on the same held-out observations.

We combine it with the pair-averaged covariance of the split-wise predictions,

$$\hat{C}_{g,k,s}^{\text{study}} = \binom{k}{2}^{-1} \sum_{a < b} \widehat{\text{Cov}}_{i \in I_{ab,s}}(g_{a,s}(x_i), g_{b,s}(x_i)), \quad (\text{D.23})$$

and with the mean pairwise out-of-fold intersection size,

$$\bar{m}_{k,s}^{\text{study}} = \binom{k}{2}^{-1} \sum_{a < b} |I_{ab,s}|. \quad (\text{D.24})$$

The early-stopping redundancy score is

$$\hat{\omega}_{k,s}^{\text{study}}(F_\lambda, n_{\text{tr}}) = \hat{C}_{g,k,s}^{\text{study}} \hat{\rho}_{e,k,s}^{\text{study}} \bar{m}_{k,s}^{\text{study}}. \quad (\text{D.25})$$

If the pairwise out-of-fold intersections are empty after only two splits, the score is simply deferred until the next split.

Mathematical intuition. The factor $\hat{C}_{g,k,s}^{\text{study}}$ measures whether the predictors trained on different splits move together on study observations. The factor $\hat{\rho}_{e,k,s}^{\text{study}}$ measures whether their out-of-fold losses move together on observations held out for both predictors. The factor $\bar{m}_{k,s}^{\text{study}}$ records how much direct overlap supports this comparison. If the product is large, repeated splits have similar prediction and error structure, so averaging more of them mostly averages redundant information and G_K^{test} should settle early. If the product is small, fold evaluations are less coupled, and additional splits can continue to reduce evaluation noise. Thus,

$$\hat{\omega}_{k,s}^{\text{study}} \text{ high} \Rightarrow \text{low or early-settling sample gain,}$$

$$\hat{\omega}_{k,s}^{\text{study}} \text{ low} \Rightarrow \text{larger sample gain remains plausible.}$$

Prospective single-run validation. We validate the rule on a prospective synthetic holdout run that was not used to derive the earlier redundancy diagnostics. This run combines 3 synthetic data families, 3 noise levels, 3 training sizes, 8 solvers, and 50 seeds, for 216 configurations and 10,800 single partial CV runs. Each run is continued to $K = 200$ splits, but the redundancy score used for triage is computed only from the first k splits of one seed.

The validation compares the single-run score $\hat{\omega}_{k,s}^{\text{study}}$ to the exact configuration-level gains G_{20}^{test} and G_{200}^{test} , computed only for analysis. These exact gains are not available to the early-stopping rule. Already at $k = 2$, the score is strongly informative: for G_{200}^{test} , the log-correlation is -0.69 and the rank correlation is -0.55 across valid partial runs. At $k = 3$, these become -0.72 and -0.59 . Using $k = 5, 10, \text{ or } 20$ changes little, showing that the triage signal appears after only a few splits.

Table D.1: Single-run early-stopping validation on the prospective synthetic holdout. Redundancy tertiles are computed from $\hat{\omega}_{k,s}^{\text{study}}$ using only the first k splits of one seed. High redundancy almost rules out large gains, while low redundancy identifies the cases where continuing CV is most promising.

Splits used	Target	Valid runs	Log corr.	Rank corr.	Median gain low/mid/high red.	Large-gain probability low/mid/high red.
2	G_{20}^{test}	9,527	-0.54	-0.45	7/5/4	$\Pr(G_{20}^{\text{test}} \geq 10) = 21.1/2.5/0.4\%$
3	G_{20}^{test}	10,441	-0.55	-0.47	7/5/4	$\Pr(G_{20}^{\text{test}} \geq 10) = 23.3/2.7/0.4\%$
2	G_{200}^{test}	9,527	-0.69	-0.55	10/6/5	$\Pr(G_{200}^{\text{test}} \geq 20) = 14.0/0.2/0.0\%$
3	G_{200}^{test}	10,441	-0.72	-0.59	10/6/5	$\Pr(G_{200}^{\text{test}} \geq 20) = 16.4/0.3/0.0\%$

This table should be read asymmetrically. A low score does not guarantee a very large gain; it only indicates that continuing is plausible. A high score is more decisive: after only two or three splits, high-redundancy runs almost never reach large gains.

For practitioners, this gives a simple early-stopping rule. Compute (D.25) after two or three splits: if redundancy is high, further CV repetitions are unlikely to pay off, even by $K = 20$; if redundancy is low, continuing to $K = 20$ is justified, and only those low-redundancy cases plausibly merit much heavier runs such as $K = 200$.

Relation with configuration-level calibration. The same qualitative relationship appears when redundancy is averaged over seeds and compared at the configuration level on the simulated-data runs used in the main analysis: high redundancy corresponds to low sample gain, and the upper tail of G_K^{test} disappears as redundancy increases. The prospective single-run validation above is the operationally relevant version of this result: it shows that the decision can be made from one partial CV run, after very few splits, without using any benchmark or outer-set observation.

E Experimental Details

E.1 Simulated data process

All simulated experiments are regression problems with normally distributed features. Each simulated dataset contains $n = 150,000$ observations in dimension $d = 5$. A held-out benchmarking set of 100,000 observations is used to estimate oracle performance, while the remaining observations form the pool from which the study and outer sets are sampled. In all simulated runs used for the redundancy analysis, each random seed regenerates the covariates, the regression coefficients, and the noise.

The baseline simulated dataset is a linear Gaussian regression. We draw $X_i \sim \mathcal{N}_5(0, I_5)$, $\beta \sim \mathcal{N}_5(0, I_5)$, and $\varepsilon_i \sim \mathcal{N}(0, 1)$ independently, and set

$$Y_i = X_i^\top \beta + \sigma \varepsilon_i.$$

The noiseless case $\sigma = 0$ corresponds to the simple model described in the main text, while the redundancy analyses also include noisy versions with $\sigma \in \{0.2, 0.5, 1\}$.

To avoid calibrating the study-only redundancy rule on a single linear data process, we also include two harder synthetic families. The first one adds all pairwise feature interactions:

$$Y_i = X_i^\top \beta + \sum_{1 \leq a < b \leq d} \gamma_{ab} X_{ia} X_{ib} + \sigma \varepsilon_i,$$

where the interaction coefficients are Gaussian and scaled by the inverse square root of the number of feature pairs. The second one is an additive nonlinear regression,

$$Y_i = \sum_{j=1}^d \beta_j \sin(4X_{ij}) + \sigma \varepsilon_i.$$

Both families are run with $\sigma \in \{0.2, 0.5, 1\}$.

E.2 Real data training loops

For both real-world dataset that we used, a global, stratified split is performed on the whole dataset. A large, held-out benchmarking set is created, comprising 244,912 in PCam and 600,000 samples in Yelp. The remaining of the data is reserved for the study set and the outer set, the latter comprising up to 200 times more images than the study test set.

To assess model performance across different data scales, we design a cross-validation protocol that operates on stratified subsets, referred to as study sets, sampled from the main study pool. The entire procedure is iterated over a predefined set of 100 random seeds for robustness.

Histopathologic scans classification The experiments on the PatchCamelyon dataset are done adapting the training script sent by the authors of the TIA Toolbox Python library.

The PCam dataset is sourced via the Hugging Face datasets library [Lhoest et al., 2021], utilizing the laurent/PatchCamelyon repository. The official training and validation splits are combined into a single unified dataset containing 294,912 histopathological images. The only preprocessing step applied is the conversion of images into PyTorch tensors.

The models used in this study are based on CNN architectures available in the torchvision library [Marcel and Rodriguez, 2010], pretrained on ImageNet [Deng et al., 2009]. For each selected architecture, the final fully-connected classification layer was removed. The pretrained convolutional

base is used as a fixed feature extractor. A new classification head is appended to this backbone, consisting of an adaptive average pooling layer followed by a single linear layer that maps the pooled features to the two output classes of the PCam dataset.

For each experimental run, defined by a specific model architecture, study set size, and random seed, the following steps are executed:

1. **Study Set Sampling:** A study set of a specific size (e.g., 1,000 or 10,000 samples) is drawn using stratified sampling to maintain the original class distribution.
2. **Fold-Level Splitting:** A CV is initiated on this study set. As the dataset is balanced, stratification is not performed. Within each fold, the data is partitioned into three distinct subsets:
 - A test set, comprising 20% of the study set’s data. This set is held out until the final evaluation for the fold.
 - A validation set, also comprising 20% of the study set’s data.
 - A training set, comprising the remaining 60% of the study set’s data.
3. **Model Training:** The CNN model is trained exclusively on the training set for a fixed number of epochs using the Adam optimizer [Kingma and Ba, 2015] and Cross-Entropy loss function.
4. **Model Selection:** After each training epoch, the model’s performance is evaluated on the validation set. The model weights that yield the highest validation accuracy across all epochs are saved as the best model for that fold.

Upon completion of training for a fold, the best-performing model is loaded and evaluated on four separate datasets:

1. The validation set for that fold.
2. The held-out test set for that fold, providing an unbiased estimate of generalization performance on the study set.
3. The outer set, also providing unbiased estimates of generalization, but on samples that are not part of the CV in that seed.
4. The global benchmarking set, providing an estimate of oracle performance on unseen data.

For each evaluation, we record the accuracy, loss, and inference runtime. All experimental parameters (model name, study size, seed, fold) and the resulting performance metrics are systematically logged. At the conclusion of all experiments, these logs are aggregated and saved into a single Parquet file for subsequent analysis.

NLP Fine-tuning The experiments on the Yelp Review Full dataset are done using an online tutorial about fine-tuning released by HuggingFace².

Within each experiment, the CV procedure is the same as the one used for PCam, detailed above.

For each CV fold, a pre-trained model is fine-tuned on the training fold. We perform full fine-tuning, where all parameters of the algorithm are updated. The training process is managed by the HuggingFace Trainer with the following hyperparameters:

- Epochs: 3
- Optimizer: AdamW [Loshchilov and Hutter, 2019] (default)
- Learning Rate: 5e-5 (default)
- Training Batch Size: 32
- Evaluation Strategy: The model’s performance on the validation fold is evaluated at the end of each epoch.
- Model Selection: The model checkpoint that achieves the highest accuracy on the validation fold is selected as the best model for that fold.

²<https://huggingface.co/docs/transformers/main/en/training>

After the training process for a single fold is complete, the best-performing model is evaluated on the validation and the benchmarking sets. The primary metric recorded for all evaluations is accuracy. We also record training and evaluation runtimes, losses, and the epoch at which the best model was found.

The script systematically iterates through a grid of experimental conditions defined by command-line arguments: model architecture, study set size, number of CV splits, random seed.

E.3 Runs and time

Table E.1: Dataset splittings in our experiments.

Dataset	Training sizes	Benchmarking size
Simulated	50; 100; 300; 1,000; 2,000	100,000
PatchCamelyon	30; 100; 300; 500; 800	244,912
Yelp Review Full	1,000; 3,000; 10,000	600,000

Table E.2: Details concerning the learning algorithms in our experiments. Displayed time values are in hours. The single-split rows aggregate the additional real-data runs used to compute the pairwise oracle ranking estimations in Table G.1.

Dataset	Learning algorithm	Hardware used	No. of seeds	No. of splits	Study time	Bench. time	Total time		
Simulated	ExtraTrees[$n_{\text{estimators}} = 200$]	AMD CPU (128 cores)	1,000	200	-	-	231.62		
	GradientBoosting[$n_{\text{estimators}} = 200$]		1,000	200	-	-	206.24		
	MLP[hidden layers = (32)]		1,000	200	-	-	192.76		
	Ridge[$\alpha = 1613$]		1,000	200	-	-	0.88		
	GradientBoosting[$n_{\text{estimators}} = 20$]		500	20	-	-	3.26		
	DecisionTree[max depth = 5]		100	20	-	-	0.04		
	DecisionTree[max depth = 20]		100	20	-	-	0.07		
	DecisionTree[max depth = 100]		100	20	-	-	0.07		
	HistGradientBoosting[max depth = 3]		100	20	-	-	0.82		
	HistGradientBoosting[max depth = 20]		100	20	-	-	2.03		
	KNeighbors[$n_{\text{neighbors}} = 5$]		100	20	-	-	0.02		
	KNeighbors[$n_{\text{neighbors}} = 20$]		100	20	-	-	0.02		
	SVR[$C = 10, \epsilon = 0.1$]		100	20	-	-	0.70		
	DecisionTree[max depth = 100]		50	200	-	-	2.11		
	HistGradientBoosting[max depth = 20]		50	200	-	-	17.97		
	KNeighbors[$n_{\text{neighbors}} = 20$]		50	200	-	-	0.07		
	RandomForest[max depth = 100, $n_{\text{estimators}} = 200$]		50	200	-	-	77.90		
	SVR[$C = 10, \epsilon = 0.1$]		50	200	-	-	14.13		
	PatchCamelyon		DenseNet121	NVIDIA V100	50	20	33.72	90.60	124.32
			MobileNetV2		50	20	25.44	74.79	100.23
ViT-B/16		50	20		121.71	1,101.76	1,223.46		
WideResNet101_2		50	20		51.27	231.68	282.95		
DenseNet121		100	1		3.76	17.87	21.62		
MobileNetV2		100	1		2.80	17.05	19.85		
WideResNet101_2		100	1		5.51	27.74	33.25		
Yelp Review Full	BERT	NVIDIA H100	50	20	112.24	325.65	437.87		
	XLM-RoBERTa		50	20	120.27	296.38	416.66		
	BERT		100	1	8.44	105.84	114.28		
	XLM-RoBERTa		100	1	8.96	105.98	114.94		

F Comparison with Repeated K -Fold

K -Fold CV uses each sample of the study set exactly once as a test sample during the procedure. This CV procedure is the most commonly used one.

We performed the exact same experiments with Repeated 5-Fold instead of MCCV. As can be observed on Figure F.1, while the variance-equivalent test sample gains appear as larger during the first 5 folds for Repeated 5-Fold compared to MCCV, this behavior does not last when K increases, ultimately yielding comparable results.

Hence, our results appear as robust when changing the CV procedure.

While K -Fold CV does not perform the resampling step described in Section 2.2, MCCV permits to dynamically estimate the study-only redundancy score defined in Section D.3.

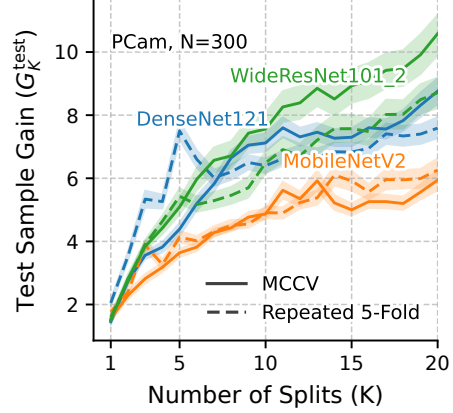


Figure F.1: Observed sample gains on PCam with training size $N = 300$ for MCCV and Repeated 5-Fold.

G Statistical Significance of Pairwise Rankings on real data

G.1 Formalization and Methodology

To rigorously compare the performance of two learning algorithms A and B , we employ a *paired t-test* across $S = 100$ independent seeds. This approach is necessary because for each seed, both algorithms are trained and evaluated on identical data splits, meaning the resulting scores are not independent.

Let $R_s^{(A)}$ and $R_s^{(B)}$ represent the benchmarking scores of the two algorithms for seed $s \in \{1, \dots, S\}$. We define the performance difference as:

$$D_s = R_s^{(A)} - R_s^{(B)} \quad (\text{G.1})$$

Our null hypothesis (H_0) and alternative hypothesis (H_1) are:

- $H_0 : \mu_D = 0$ (There is no significant difference in performance).
- $H_1 : \mu_D \neq 0$ (The performance difference is statistically significant).

G.2 Calculus and Estimators

The mean difference \bar{D} and the sample standard deviation s_D are computed from the S experimental runs:

$$\bar{D} = \frac{1}{S} \sum_{s=1}^S D_s, \quad s_D = \sqrt{\frac{1}{S-1} \sum_{s=1}^S (D_s - \bar{D})^2} \quad (\text{G.2})$$

Under the Central Limit Theorem, the test statistic t follows a Student's t-distribution with $df = S - 1$ degrees of freedom:

$$t = \frac{\bar{D}}{s_D / \sqrt{S}} \quad (\text{G.3})$$

We evaluate significance at the $\alpha = 0.05$ level. For $df = 99$, the two-tailed critical value is $t_{crit} = 1.9842$. A result is considered statistically significant if $|t| > t_{crit}$, or equivalently, if the p -value < 0.05 .

Table G.1: Paired t-test results on real datasets comparing mean benchmarking differences over $S = 100$ paired seeds. Significant results ($p < 0.05$) are highlighted. The last two columns report the proportion of paired runs retrieving the displayed oracle direction with a single split and with $K = 20$ CV; the CV column uses the available 20-split CV runs.

Highest Mean	Lowest Mean	Training Size (N)	Mean Diff (\bar{D})	Std Dev (s_D)	t -stat	p -value	Single-Split Retrieval	$K = 20$ CV Retrieval
PatchCamelyon								
DenseNet121	MobileNetV2	30	0.04724	0.07367	6.413	< 0.0001	49%	56%
DenseNet121	WideResNet101_2	30	0.04214	0.09117	4.622	< 0.0001	40%	74%
WideResNet101_2	MobileNetV2	30	0.00510	0.09013	0.566	0.5725	32%	36%
DenseNet121	MobileNetV2	100	0.00335	0.08558	0.391	0.6967	39%	60%
DenseNet121	WideResNet101_2	100	0.06279	0.07666	8.191	< 0.0001	60%	100%
MobileNetV2	WideResNet101_2	100	0.05945	0.07987	7.443	< 0.0001	61%	96%
MobileNetV2	DenseNet121	300	0.01083	0.04034	2.686	0.0085	45%	82%
DenseNet121	WideResNet101_2	300	0.05056	0.05508	9.179	< 0.0001	71%	96%
MobileNetV2	WideResNet101_2	300	0.06140	0.04572	13.429	< 0.0001	79%	100%
MobileNetV2	DenseNet121	500	0.00110	0.02114	0.520	0.6044	45%	70%
DenseNet121	WideResNet101_2	500	0.04421	0.03556	12.432	< 0.0001	76%	100%
MobileNetV2	WideResNet101_2	500	0.04531	0.03755	12.068	< 0.0001	76%	100%
MobileNetV2	DenseNet121	800	0.00223	0.01750	1.276	0.2050	47%	54%
DenseNet121	WideResNet101_2	800	0.04186	0.02407	17.394	< 0.0001	84%	100%
MobileNetV2	WideResNet101_2	800	0.04409	0.02388	18.466	< 0.0001	85%	100%
Yelp Review Full								
BERT	XLm-RoBERTa	1,000	0.04793	0.08505	5.636	< 0.0001	70%	92%
BERT	XLm-RoBERTa	3,000	0.01959	0.10158	1.919	0.0579	30%	51%
BERT	XLm-RoBERTa	10,000	0.00803	0.10029	0.801	0.4251	11%	58%

G.3 Empirical Results

G.3.1 Medical Imaging

Table G.1 presents the comparative analysis of our experimental results.

The analysis reveals a stable separation between WideResNet101_2 and the two other CNN architectures once $N \geq 100$: both DenseNet121 and MobileNetV2 significantly outperform it at every such training size. At the smallest training size, $N = 30$, DenseNet121 significantly outperforms both MobileNetV2 and WideResNet101_2, while the difference between WideResNet101_2 and MobileNetV2 is not significant. From $N = 300$ onward, MobileNetV2 has the highest mean benchmarking score. Its advantage over DenseNet121 is significant at $N = 300$, but no longer significant at $N = 500$ or $N = 800$. This suggests that DenseNet121 is preferable in the lowest-data regime, whereas MobileNetV2 and DenseNet121 become statistically close at larger training sizes.

It is important to note the role of the benchmarking set size ($B = 244,912$). In a binomial classification task, the variance of the accuracy estimator attributed to the test set size is bounded by $\frac{1}{4B}$. Given our large B , this bound of the variance is $\approx 1.02 \times 10^{-6}$, corresponding to a standard deviation of at most ≈ 0.00101 , which is an order of magnitude smaller than the observed sample standard deviation s_D .

Consequently, the benchmarking size B ensures that the standard deviation s_D reported in Table G.1 is mostly measuring the algorithms’ sensitivity to the training data composition and split seed, rather than noise from the finite benchmarking set. This high-fidelity evaluation strengthens the reliability of the p -values calculated.

G.3.2 NLP Fine-Tuning

Here, we apply the paired t-test methodology to evaluate the performance differences between BERT and XLm-RoBERTa architectures. For this dataset, models were evaluated on a benchmarking set of size $M = 600,000$. The extremely large size of M ensures that the standard error of the evaluation metric is negligible, meaning the observed variance s_D is a direct reflection of model instability across training subsets. Table G.1 summarizes the findings for three training scales. Notably, as the training size N increases, the mean difference \bar{D} decreases, while the standard deviation s_D remains relatively high, suggesting that both models exhibit significant sensitivity to the training seed in this specific task.

The analysis indicates that BERT is significantly superior to XLM-RoBERTa at the smallest experimented training scale ($N = 1000, p < 0.0001$). However, this advantage vanishes as more data is provided:

- At $N = 3000$, the difference is only marginally significant ($p = 0.0579$), failing to reach the standard $\alpha = 0.05$ threshold.
- At $N = 10000$, the models are statistically indistinguishable ($p = 0.4251$), with the mean difference falling well within the noise floor generated by the training seeds.

This suggests that XLM-RoBERTa’s performance catches up to BERT’s as the sample size increases, and any observed difference at $N = 10000$ is likely due to random chance in the training data selection rather than a structural superiority of one architecture over the other.

H Varying training size: Ranking-Equivalent Sample Gain

In the synthetic experiments, the oracle ranking is stable across the study sizes we consider. This makes it possible to ask a complementary question: how much can increasing the number of partitions reduce the study size needed to recover the oracle ranking with high probability?

From score variance to ranking reliability Consider a family of M learning algorithms with distinct oracle scores at training size n_{tr} , indexed without loss of generality in oracle order $F_1 \succ F_2 \succ \dots \succ F_M$. For a study set of size N and a CV procedure with K splits, let $\widehat{R}_K(F_m; N)$ be the MCCV estimator of F_m , all computed on the same splits (paired). We say the *full ranking* is recovered when the empirical order of the whole family matches the oracle order, and define the ranking-retrieval probability

$$\pi_K(N) = \mathbb{P}\left[\widehat{R}_K(F_1; N) \succ \widehat{R}_K(F_2; N) \succ \dots \succ \widehat{R}_K(F_M; N)\right], \quad (\text{H.1})$$

where \succ denotes the same ordering convention as the oracle ranking (loss vs. utility). This probability is monotone non-decreasing in both N and K when score variance dominates the comparison, and tends to 1 as either grows.

The reasoning of [Section 3](#) can then be transposed from score variance to ranking reliability: rather than asking how much extra test data a single hold-out would need to match the variance of a K -split estimator, we ask how much smaller a study set K -split CV needs to reach a given full-ranking-retrieval level relative to a single hold-out.

Definition H.1 (Threshold-Crossing Study Size). For a family of algorithms with a fixed oracle ranking, a CV procedure with K splits, and a confidence level $\alpha \in (\frac{1}{2}, 1)$, the *threshold-crossing study size* is the smallest study size at which the full oracle ranking is recovered with probability at least α :

$$N_{K,\alpha}^* = \min\left\{N \geq 1 \mid \pi_K(N) \geq \alpha\right\}. \quad (\text{H.2})$$

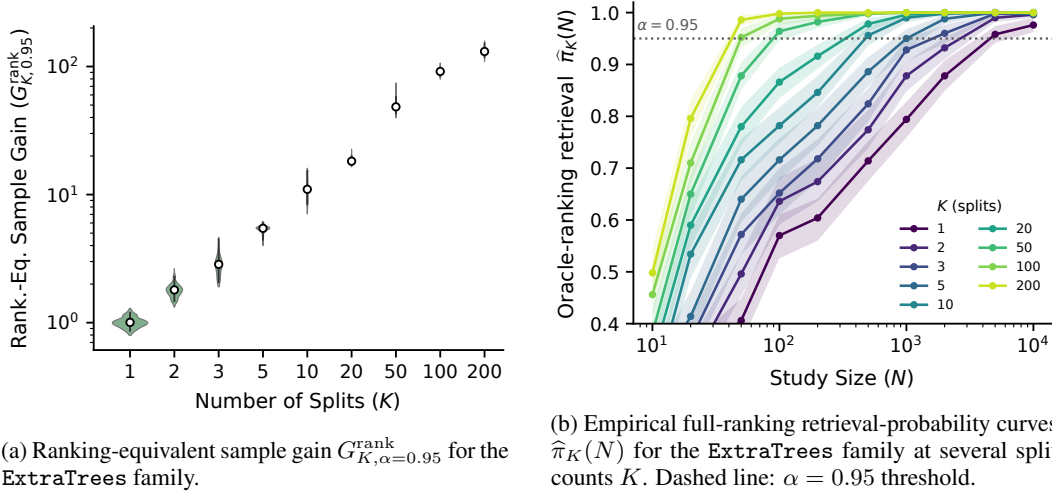
By the monotonicity of π_K in N , this size is well-defined as soon as α is reachable. In practice it is read off an empirical retrieval-probability curve $\widehat{\pi}_K(N)$ at the level α (typically $\alpha = 0.95$), as illustrated in [Figure H.1b](#).

Definition H.2 (Ranking-Equivalent Sample Gain). The **ranking-equivalent sample gain** of a K -split CV procedure is the ratio of the single-split threshold-crossing size to the K -split threshold-crossing size:

$$G_{K,\alpha}^{\text{rank}} = \frac{N_{1,\alpha}^*}{N_{K,\alpha}^*}. \quad (\text{H.3})$$

A value $G_{K,\alpha}^{\text{rank}} = 10$ indicates that, for the family at hand, K -split CV recovers the full oracle ranking at the α retrieval level with a study set ten times smaller than the one a single hold-out would require. By construction $G_{1,\alpha}^{\text{rank}} = 1$, and the gain is non-decreasing in K whenever π_K is non-decreasing in K . In practice, π_K is estimated by the empirical full-ranking retrieval proportion across independent seeds, and the two threshold-crossing sizes in [\(H.3\)](#) are read off the single-split and K -split retrieval curves at level α ([Figure H.1b](#)). The distribution of $G_{K,\alpha}^{\text{rank}}$ reported in [Figure H.1a](#) is obtained by a non-parametric bootstrap over seeds, recomputing $N_{K,\alpha}^*$ on each resample while holding the numerator $N_{1,\alpha}^*$ at its population value.

A family with a known oracle ranking Computing $G_{K,\alpha}^{\text{rank}}$ requires knowing the full oracle ranking of the family. To guarantee this without relying on benchmark-set estimates, we construct families in which the ordering is fixed by design, by varying a single hyperparameter that monotonically orders the oracle risk: for Ridge, the regularization strength α (under the simulated linear data process of Appendix E, larger α induces more bias and monotonically degrades the oracle risk), and for ExtraTrees, the number of estimators $n_{\text{estimators}}$ (more estimators monotonically reduce the oracle risk through ensemble averaging). We illustrate with the ExtraTrees family ($n_{\text{estimators}} \in \{2, 20, 200\}$, oracle order $n_{\text{estimators}} = 200 \succ 20 \succ 2$): the full oracle ordering of its three members is pinned by the hyperparameter ordering, so the empirical full-ranking retrieval proportion $\hat{\pi}_K(N)$ — and hence $G_{K,\alpha}^{\text{rank}}$ — is well-defined without any benchmarking-set estimate of $\mathcal{R}_{n_{\text{tr}}}^*$.



(a) Ranking-equivalent sample gain $G_{K,\alpha=0.95}^{\text{rank}}$ for the ExtraTrees family.

(b) Empirical full-ranking retrieval-probability curves $\hat{\pi}_K(N)$ for the ExtraTrees family at several split counts K . Dashed line: $\alpha = 0.95$ threshold.

Figure H.1: Ranking-equivalent sample gain on the simulated regression task for the ExtraTrees family, whose oracle order ($n_{\text{estimators}} = 200 \succ 20 \succ 2$) is fixed by hyperparameter monotonicity. (a) Distribution of $G_{K,\alpha=0.95}^{\text{rank}}$ across K , with the spread obtained by a non-parametric bootstrap over seeds. (b) Full-ranking retrieval-probability curves $\hat{\pi}_K(N)$ as a function of study size N , for several split counts K . The minimum study size at which each curve crosses the $\alpha = 0.95$ threshold is the empirical analogue of $N_{K,\alpha}^*$ used to compute the gain in (a) (the $K = 1$ curve providing the numerator).

Figure H.1a shows that recovering the full oracle ranking benefits markedly from additional splits: even $K = 10$ partitions already multiply the effective study size roughly tenfold, and the gain keeps climbing steeply with K , reaching close to two orders of magnitude by $K = 200$. The effect continues well beyond the first few folds, again indicating that the “each observation has been held out once” heuristic is too conservative for ranking-oriented benchmarks. The retrieval-probability curves in Figure H.1b make the construction concrete: each K -curve crosses the $\alpha = 0.95$ threshold at its own $N_{K,\alpha}^*$, and the gain is the ratio of these threshold-crossing study sizes relative to the $K = 1$ curve. The gain is not linear in K , but the improvement remains visible well past $K = 5$. Thus, for ranking-oriented benchmarks, the number of splits should be chosen as a statistical-computational trade-off rather than fixed by the traditional single-pass intuition.

This quantity is complementary to G_K^{test} : it does not measure the variance of a score estimator directly, but the study size needed to make the ranking decision reliable. The same qualitative message appears in both views. Additional splits remain useful when they reduce the instability of the benchmark statistic that ultimately determines the scientific claim. This appendix is not meant to replace the main-paper test sample gain. Instead, it illustrates that the same variance-reduction mechanism can be expressed in different units: additional test samples for score estimation, or additional study samples for ranking recovery. Both views point to the same operational recommendation: use as many splits as the computational budget permits when the benchmark data are scarce and the target comparison is close.